2016

ELECTRON BEAM INDUCED DEPOSITION OF HIGHLY CONDUCTIVE COPPER NANOWIRES FROM BULK LIQUIDS

Amjad M. Syam

University of Kentucky, amjad.siam@gmail.com
Author ORCID Identifier:
 http://orcid.org/0000-0003-3839-6058
Digital Object Identifier: https://doi.org/10.13023/ETD.2016.510

STUDENT AGREEMENT:

I represent that my thesis or dissertation and abstract are my original work. Proper attribution has been given to all outside sources. I understand that I am solely responsible for obtaining any needed copyright permissions. I have obtained needed written permission statement(s) from the owner(s) of each third-party copyrighted matter to be included in my work, allowing electronic distribution (if such use is not permitted by the fair use doctrine) which will be submitted to UKnowledge as Additional File.

I hereby grant to The University of Kentucky and its agents the irrevocable, non-exclusive, and royalty-free license to archive and make accessible my work in whole or in part in all forms of media, now or hereafter known. I agree that the document mentioned above may be made available immediately for worldwide access unless an embargo applies.

I retain all other ownership rights to the copyright of my work. I also retain the right to use in future works (such as articles or books) all or part of my work. I understand that I am free to register the copyright to my work.

REVIEW, APPROVAL AND ACCEPTANCE

The document mentioned above has been reviewed and accepted by the student's advisor, on behalf of the advisory committee, and by the Director of Graduate Studies (DGS), on behalf of the program; we verify that this is the final, approved version of the student's thesis including all changes required by the advisory committee. The undersigned agree to abide by the statements above.

<div align="right">

Amjad M. Syam, Student

Dr. J. Todd Hastings, Major Professor

Dr. Cai-Cheng Lu, Director of Graduate Studies

</div>

ELECTRON BEAM INDUCED DEPOSITION OF HIGHLY CONDUCTIVE
COPPER NANOWIRES FROM BULK LIQUIDS

THESIS

A thesis submitted in partial fulfillment of the requirements for the
degree of Master of Science in Electrical Engineering in the
College of Engineering at the University of Kentucky

By
Amjad Syam
Lexington, Kentucky

Director: Dr. J. Todd Hastings, Professor of Electrical Engineering
Lexington, Kentucky

2016

ABSTRACT OF THESIS

ELECTRON BEAM INDUCED DEPOSITION OF HIGHLY CONDUCTIVE
COPPER NANOWIRES FROM BULK LIQUIDS

Electron-beam induced deposition (EBID) is a position-controlled technique that can directly fabricate nanometer-sized structures in functional materials. In the standard process, a gaseous precursor delivers the desired substance to the substrate for deposition. However, the material purity from these precursors is typically poor, which often negatively affects the functional properties of the deposit. Recently, bulk liquid precursors have been investigated as promising reactants for high purity deposition without the need for post-processing. In this work, EBID from bulk liquids is shown to yield highly conductive nanowire deposits. Aqueous solutions containing copper sulfate ($CuSO_4$) and sulfuric acid (H_2SO_4) are used as precursors to deposit copper nanowires on oxidized silicon substrates in an environmental scanning electron microscope (ESEM). Using four point I-V measurement, our results show a copper resistivity as low as 67 $\mu\Omega\bullet$cm, which is 6-8 orders of magnitude lower than that of as-deposited copper from gas phase reactants, 4-5 orders of magnitude lower than that of annealed materials, and within 1 order of magnitude of bulk copper. The low resistivity of these deposits without post-processing highlights the importance of further research to overcome challenges associated with deposition via liquid precursors, such as collateral deposition; local delivery of the reactant; and control of liquid thickness.

KEYWORDS: EBID, LP-EBID, copper nanowires, resistivity, liquid precursor, $CuSO_4$.

Author's Signature:_____Amjad Syam

Date:_____December 9, 2016

ELECTRON BEAM INDUCED DEPOSITION OF HIGHLY CONDUCTIVE
COPPER NANOWIRES FROM BULK LIQUIDS

By

Amjad Syam

Director of Thesis: <u>J. Todd Hastings</u>

Director of Graduate Studies: <u>Cai-Cheng Lu</u>

Date: <u>12/09/2016</u>

To my mother, father, and family, who always kept me in their thoughts and prayers; and to Noora Aljabi, my best friend and partner in life.

ACKNOWLEDGEMENTS

My deepest gratitude goes to my advisor, family, wife, and friends, whose support, help, and guidance aided me to reach this point in my life.

I would like to express my fullest appreciation of my advisor, Dr. Hastings, for his guidance, optimism, patience and availability anytime I needed him.

I would like to thank Dr. Vijay Singh and Dr. Janet Lumpp for accepting to be on my thesis defense committee and for their valuable feedback and support.

Special thanks and gratitude to my previous and current colleagues, Adham Noubani, Alex Burkhart, Lindsay Boehme, Mansoor Sultan, Samaneh Esfandiarpour, Sarah Lami, Gabriel Smith, for providing their assistance with the experimental work, their motivation and encouragement during down times, and for being excellent company.

I would like to thank Mr. Brain Wajdyk, and Jacob Hempel for the technical support, training, availability, and guidance at Center for Nanoscale Science and Engineering (CeNSE).

Technical support was also provided by the staff of the Electron Microscopy Center. Special thanks to Nicolas Briot and Azin Akbari for their assistance with equipment logistics.

I would like to thank Dr. Douglas Strachan for making the electron beam evaporator in his lab available for my use. I would also like to thank Mohsen Nasseri from the Physics department for his assistance, time and effort in operating the electron beam evaporator.

Special thanks to FEI for supplying the Liquid Injection System (LIS). I want to also extend special thanks and gratitude to Aurélien Botman for his guidance and advice on using the LIS.

Finally, and most importantly, I want to express my thankfulness for my mother, father, family, friends, and my wife Noora for always supporting me in my life and for being there when I needed them the most.

TABLE OF CONTENTS

v

LIST OF TABLES

LIST OF FIGURES

Chapter 1: Introduction

1.1 Importance of Liquid-Phase Electron Beam Induced Deposition (LP-EBID)

Some of the challenges that are facing the Integrated Circuit (IC) industry nowadays are the ability to do fast and inexpensive circuit edit, device prototype, and easy three-dimensional micro-nanostructures. In addition, the relatively time consuming and high repair costs of ICs affect its throughput, and call for effective patterning techniques that address these challenges. One such technique that has been investigated for a while is Electron Beam Induced Deposition (EBID). EBID is a direct nano-scale patterning technique that allows the deposition of functional materials via gaseous precursors. EBID has been investigated for various applications including direct interconnect fabrication (carbon,[1] platinum,[2] gold,[3] and many other materials [4-6]) photolithographic mask repair [7], growth of deterministic catalyst material [5], Field emission devices [8], and optical applications [9]. However, many of these gaseous precursors are toxic in nature, expensive and difficult to deal with. Furthermore, perhaps the most important issue with the use of gaseous precursors in EBID is the relatively low purity achieved deposits [10-12], which is the main limiting factor in EBID applications [13].

This issue becomes apparent with interconnect fabrication/repair. Traditionally, Aluminum alloys dominated the interconnect domain, however, with the current progress of circuit miniaturization, interconnects are facing higher current densities, which could impact their overall lifetime due to issues such as electromigration. Since Aluminum alloys are highly susceptible to electromigration, copper has been considered as a possible replacement for interconnects due to its high conductivity and resilience to electromigration. Since copper deposition from EBID has been shown to be highly resistive [11, 12], EBID is therefore limited in that industry. This calls for a more refined patterning technique to overcome the issue of low conductivity of copper deposits from EBID.

Liquid-phase electron beam induced deposition (LP-EBID) is currently being studied as a maskless, resistless, 3-D *high purity* nano-scale patterning technique that renders the direct deposition of functional materials. The significance of LP-EBID comes from the

use of liquid precursors as mediums for deposition, as opposed to gaseous precursors which are used in EBID. Liquid precursors have been shown to produce high purity content deposits [14-16], especially for copper [17, 18], and holds promise for a wide variety of benign and inexpensive precursors. The goal of this work is to quantify the resistivity of copper nanowires deposited via LP-EBID and compare it to previous copper resistivity results in the literature of EBID. Given the obtained positive results, LP-EBID has the potential to advance existing EBID applications such as IC processes such as interconnects, circuit edit, rapid device prototyping, as well as open new doors in the field of nanofabrication.

1.2 Overview of chapters

This thesis will consist of five chapters. Following this introductory chapter, chapter two will focus on reviewing the available literature on EBID. First, a brief historical background of EBID is provided that highlights the first observations of EBID. Then, a summary on the process of EBID will demonstrate how EBID works on a higher level. Following that, a review on the applications of EBID in the literature will be provided that will accentuate the utilization of EBID across many fields. This will lead into a discussion of some of the issues with EBID that have surfaced across the literature, of which a focused discussion on the purity and metal resistivity limitations of EBID deposits will follow. Next, I will review previous attempts at EBID deposit purification and pave the way to introduce LP-EBID as a promising technique for high purity deposition. The chapter will end with a discussion on the advantages and limitation of LP-EBID.

Chapter three will narrow the discussion on the importance of copper and provide justification for the choice of copper in this work. This will lead to a review and discussion of copper precursors in EBID literature in terms of obtained purity. Finally, a review on copper precursors in LP-EBID will highlight the improved material purity as well as the motivation behind quantifying the resistivity of LP-EBID deposits.

Chapter four will provide detailed description of the experimental process of LP-EBID and of the process to obtain resistivity values for the deposits. The starting materials,

sample preparation, deposition process, and extraction of resistivity values will be illustrated and detailed.

Finally, chapter five will present the LP-EBID structures along with their extracted resistivities, followed by a discussion of the obtained results and a comparison with previous results from the literature. Challenges and issues that arose during this study will be highlighted and addressed. Finally, chapter five will conclude this work with final remarks and calls for further research in LP-EBID.

Chapter 2: Electron Beam Induced Deposition

2.1 Historical background

One of the first noticed incidences of EBID was in 1933, where carbonaceous deposits were seen to grow as a result of ion-bombardment to contaminated surfaces [19]. However, the author considered these deposits a source of error. This phenomenon was believed to be a result of some sort of interaction between the ion/electron beam and organic vapor present in the vacuum chamber. This organic vapor, or source of contamination, was believed to come from poor vacuum in microscope chambers, as well as residual oil from diffusion pumps and vacuum grease. Several methods to limit the growth of these carbonaceous insulating films, i.e. reduce sample contamination inside microscope chambers, were presented in later years [20]. It wasn't until the 1960s that this phenomenon was exploited to grow insulating layers where needed, such as organic silicon polymers for dielectric film growth [21].

Up to this point, EBID was still not given too much attention. According to Silvis-Cividjian's review of EBID [22], it was in 1976 that Broers fabricated 80 Angstrom metal lines using a condensed hydrocarbon vapor as a negative resist [23]. Afterwards, contamination lithography, as it was called, proved to be a highly successful technique to produce high-resolution features. Consequently, hydrocarbon vapors and organometallic precursors started to be intentionally introduced in focused beam systems in order to study electron/ion beam induced processes – EBIP/IBIP [22].

This thesis is not meant to give an exhaustive historical review of EBID. There are other reviews that provide more details on the history of EBID as well as its governing principles. Silvis-Cividjian provides a more comprehensive historical background on EBID and an in-depth discussion on the theory of EBID spatial resolution [22]. Van Dorp et al. sorts and categorizes the literature on the effects of varying beam parameters, such as current density, accelerating voltage, etc) on the properties of the deposits, such as composition, morphology and conductivity [13]. Rack et al. provides a good introduction to EBID and Electron Beam Induced Etching (EBIE), as well as provide a summary on the physics associated with electron-solid-vapor interactions and discuss specific application of e-beam induced processes [24].

2.2 EBID process

As mentioned in the previous section, EBID was believed to occur as a result of some sort of interaction between an electron beam and organic vapor present in the vacuum system. Indeed, if, for example, an organometallic precursor is adsorbed on the surface of a substrate that is being irradiated by an electron beam, then the e-beam dissociates the precursor molecules into volatile and non-volatile byproducts as a result of inelastic scattering of the electrons with the precursor molecule. Thus far, it is not clear whether dissociation occurs due to high energy electrons (i.e. primary electrons) or low energy electrons (i.e. secondary electrons emitted from the surface), or both. Nevertheless, the volatile byproducts desorb from the surface of the substrate, leaving behind non-volatile solids adhered to the substrate. Of course, the chemistry of the precursor, along with beam parameters and many other factors, govern the composition of the volatile and non-volatile components; Furthermore, this effect occurs only around the e-beam irradiated area, which makes EBID a highly localized deposition technique. Figure (2-1) illustrates the process of EBID. For a more in-depth discussion of dissociation processes, refer to [13]. An electron beam can also interact with a precursor to etch material away. The process is called Electron Beam Induced Etching (EBIE). EBID combined with EBIE are typically referred to as Electron Beam Induced Processes (EBIP).
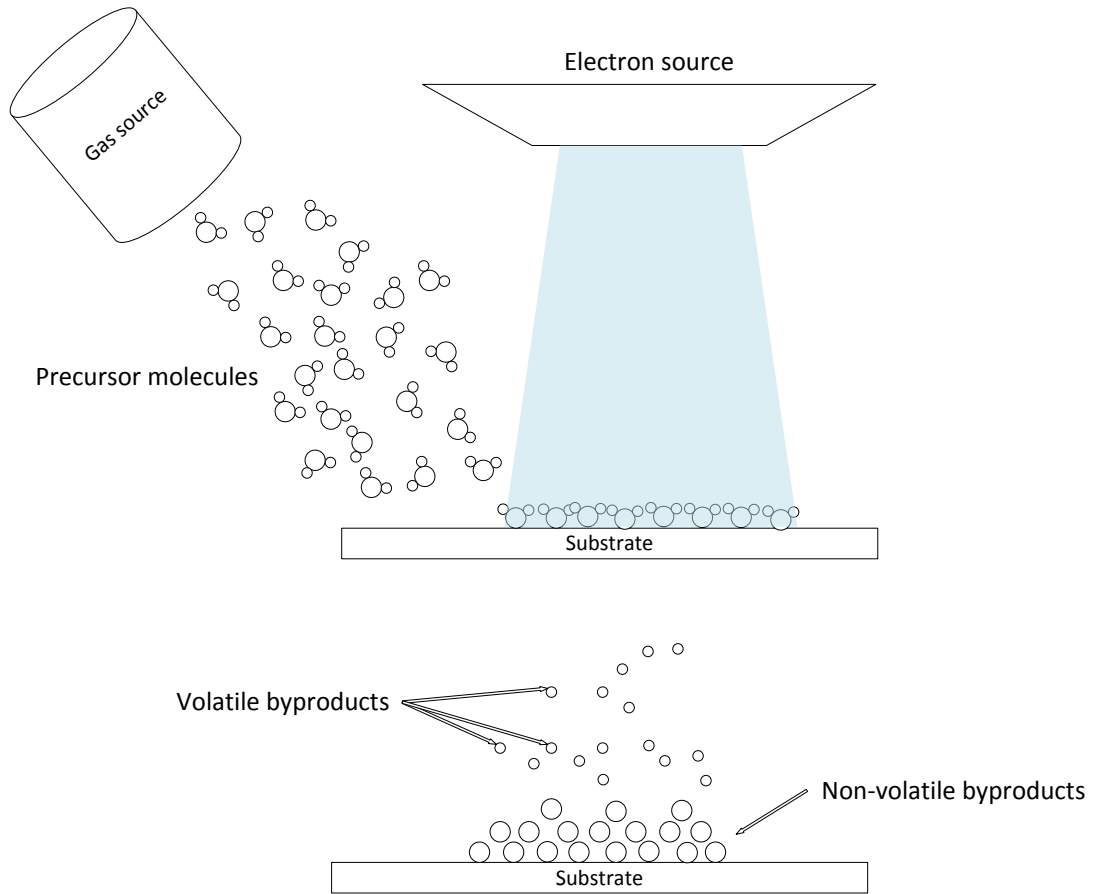
Figure 2-1: Illustration of EBID process. A gas source injects a precursor into the chamber of a scanning electron microscope, where the beam interacts with the precursor molecules to induce dissociation. Non-volatile byproducts stick on the surface of the substrate, whereas voltile byproducts are pumped away.

2.3 Applications of EBID

As EBID evolved over the past 30 years, it has become one of the most useful deposition techniques due to its ability to perform localized, maskless, and resistless deposition of functional materials. As research groups investigated the processes behind EBID, many of its practical applications surfaced. One of the applications of EBID is direct interconnect fabrication. Silvis-Cividjian investigated interconnect fabrication of carbon in order to further understand the limitations of EBID feature size [1]. Gopal et al. studied the electrical and microstructural organization of EBID of platinum interconnect deposits [2]. In addition to carbon and platinum, other groups demonstrated interconnect

fabrication of copper [25], gold [3], nickel [4], cobalt [5], Tungsten [6], and many more. Across these publications, different parameters of deposition were varied, such as beam energy, current, dose, scan speed, and chamber gas, in order to investigate important properties of the deposits, such as resistivity, purity, morphology, composition, and structural strength.

EBID was not only utilized in interconnect fabrication. It was also seen in photolithographic mask repair [7]. Photomasks are usually very expensive to produce, and their manufacturing process is prone to yield defect masks. EBID provides a means for localized addition of material, hence, it can be used to repair defect photomask at a fraction of the price of making a new mask. Furthermore, EBID has been shown to repair some types of masks that would be difficult to repair using conventional methods for reasons such as FIB (ion contamination), laser ablation, and mechanical nanomachining. Other EBID applications include growth of deterministic catalyst material [5], Field emission devices [8], and optical applications [9].

An example of an EBID deposit is shown in figure (2-2). The study highlights the effect of scan direction on growth rate of the deposited structures. The growth rate increases as the scan progresses towards the gas injection needle, which introduces a copper precursor into the chamber. This figure is also a good example that illustrates the ease of obtaining 3D structures from EBID.
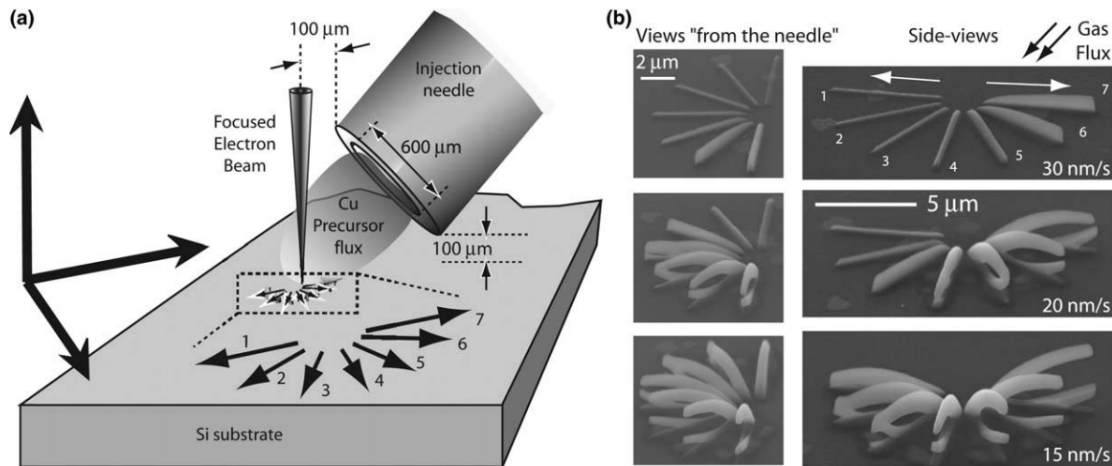
Figure 2-2: Illustration of direction dependent growth rate of EBID deposits [26].

2.4 Issues of EBID

As with any technology that attracts a lot of research, EBID presented limitations that require further studies to overcome. This section will shed some light on a few of these limitations.

Up until [1] was published, efforts around EBID had only yielded 15-20 nm structures, and little knowledge was available on the reason behind this limitation, given that the probe sizes of Scanning Electron Microscopes (SEMs) and Scanning Transmission Electron Microscopes (STEMs) are much smaller than that. It turns out that during the first stages of deposition, the secondary electrons, emitted from the primary electrons hitting the substrate, determine the lateral size of the deposit. However, as the structure grows, the lateral broadening of structure is caused by extra deposition from secondary electrons emitted from the structure itself. This introduces a limitation on structure size fabricated by EBID, in that structures would always be bigger than the beam diameter.

In [2], the authors found that there was significant leakage current around deposited platinum structures that was proportional to the beam energy. Their conclusion was that some of the deposited metal delocalized during deposition and re-adhered to the substrate away from the deposit. It turns out that, in addition to lateral broadening of structures due to secondary electrons, there was a thermally assisted diffusion component that drove the delocalized platinum away from the deposit. The spread was found to be a strong function of the electron beam energy. This meant that caution is needed when depositing interconnects in nanoelectronics, and lower beam energies are to be used during deposition in order to reduce leakage current around deposited interconnects.

Aside from the fidelity and leakage current issues, one of the major, if not the most important, limitation that keeps appearing across the various papers on EBID is the purity and electrical resistivity of the deposits. As mentioned in [13], the main limiting factor in all EBID applications is the relatively low purity content of the deposited material. For example, recent studies on the resistivity of platinum from EBID have been able to achieve on the order of $\sim 10^7 \mu\Omega\bullet$cm [27] where the resistivity of bulk platinum is 10.6 $\mu\Omega\bullet$cm. Similarly, conventional EBID of gold yields 10^8 $\mu\Omega\bullet$cm [27], copper 10^{10} $\mu\Omega\bullet$cm [11, 12], and tungsten $\sim 10^4$ $\mu\Omega\bullet$cm [28]. Compared to their bulk resistivity, it

becomes apparent that this is an extremely important problem, since highly resistive material not only reduces the electrical performance of the deposits, but also dissipates more power and induces heating which can strain the structural dynamics of the deposits. The causes behind low purity content in EBID generally stem from two factors: (1) Contamination from Chamber gas and (2) Decomposition nature of the precursor molecule (partial or incomplete dissociation) [27]. The next section will provide a brief review on some attempts at deposit purification.

2.5 Attempts at deposit purification

In [27], the study proposed several purification techniques to reduce contamination levels from gaseous deposits. One technique involves annealing the deposits onto a hot substrate during deposition. The hot substrate is used to reduce the residence time of impurities after precursor dissociation on the surface of the substrate, therefore preventing the inclusion of impurities as the material grows. One drawback to this purification technique is the reduced deposition yield due to the lower surface residence time of the precursor on the hot substrate. Alternatively, annealing could be carried out after deposition. Applying heat to deposited structures could induce recrystallization of the metal and remove carbon, thus improving the purity and resistivity of the deposits. The problem with this technique is that as the carbon is removed from the volume of the deposit, the final geometry of the deposit undergoes certain distortions. Furthermore, by applying heat, there is always the risk of forming alloys or silicides, which is often undesirable.

Rack et al. demonstrated a novel annealing technique that not only purifies the deposits, but also bypasses some of the issues associated with conventional annealing methods mentioned above [29]. The technique involves cyclic deposition/laser heating of the deposits, called Laser Assisted Electron Beam Induced Deposition (LAEBID). The idea is to apply heat on a layer-by-layer basis as the deposit grows. This has been shown to improve the deposition yield, and reduce geometrical distortions as the contaminants are removed while the deposits grow.

Ion Beam Induced Deposition (IBID) has been shown to decrease the carbon contamination in deposits [27]. IBID helps reduce carbon contamination since ions

9

provide a larger cross section for dissociation of precursor molecules, as well as higher component splitting per reaction due to the larger mass of the ions. The issue with this technique is that IBID tends to adds ion contamination around the deposition area. In addition, it tends to damage the surface of the substrate, and reduce the deposition resolution.

Ultra-High Vacuum set-ups can also be used to reduce contamination in the deposits and increase their conductivity. As mentioned before, part of the contamination in the deposit may come from residual gas in the chamber; reducing the chamber pressure, typically to 10^{-9} torr, obviously reduces the residual gas levels in the chamber, lowering the probability that a contaminant molecule interacts with the beam. Also, reducing the chamber pressure lowers the presence of water vapor in the chamber, which could lower the rate of metal oxidation provided the metal is susceptible to oxidation. In the case that a UHV setup is not available, then working clean and performing a chamber plasma cleaning process can help reduce the carbon content inside the chamber [27].

Other groups addressed the issue with EBID purity by modifying the composition or nature of the precursors through additives either before or during deposition. Recently, highly conductive and almost pure gold was deposited via EBID by using a commercial organometallic precursor for gold and water as an oxidative enhancer [30]. The study was able to increase the content of gold from a conventional 25 at.% to 91 at.% by simply injecting water at the same time with the precursor during deposition. The water would react with the carbon (and carrier gas) in the precursor to reduce the volume of deposited carbon and free up more surface sites for gold to be deposited. The results were highly conductive gold with almost bulk resistivity. However, this process has not been shown to deposit other, more oxidation-prone materials like copper, iron, and chrome.

One particularly important and effective approach at achieving highly pure EBID deposits was the introduction of liquid precursors as mediums for deposition instead of gaseous precursors. This will be discussed in the next section.

2.6 Liquid-Phase Electron Beam Induced Deposition – LP-EBID

In 2009, Donev and Hastings demonstrated the first EBID from a liquid precursor [14]. The study showed deposition of highly pure platinum that is free from carbon contamination (~10 at.% chlorine contamination versus 40-65 at.% carbon contamination from commercial Pt precursors) with deposition rates much faster than conventional EBID. This finding was important not only for the improved purity of the deposits, but also because it later opened the door for deposition of materials that had either no gas carrier – such as silver – or highly unstable precursors – such as copper.

Several studies investigated EBID via bulk liquids, where the electron beam can be focused on a thin layer of liquid precursor to dissociate precursor molecules and deposit desired materials. EBID from bulk liquids took form in the following three methods. The first was using a liquid cell, or capsule, that is coated with an electron transparent layer placed in a high vacuum chamber [14, 31]. The second involved ex-situ introduction of precursor solution, where hydration of solidified precursor can then occur in-situ in low vacuum environments [16]. The third method introduced an in-situ liquid injection system, where a microscopic precursor droplet is stabilized by controlling the droplet evaporation rate with the substrate temperature and the pressure of H2O vapor injected into the vacuum chamber [32]. Following is a discussion and illustration of each methodology.
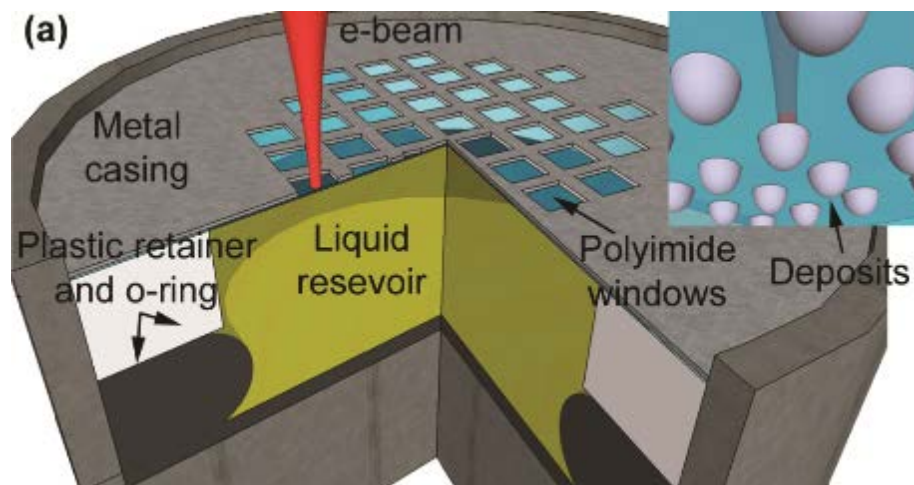
Figure 2-3: Illustration of a liquid cell [15]. Inset: Deposits form on the liquid side of the cell.

Figure (2-3) shows an example of a liquid cell intended to store liquid precursors inside a high vacuum chamber. The square, polyimide-covered windows represent entry points for an electron beam to penetrate the cell and induce deposition on the liquid side. The inset illustrates deposited material after the e-beam interacts with the precursor. Many of the early experimental work on LP-EBID used these liquid cells extensively to investigate the interaction between electrons and liquid precursors, as well as the process behind the formation and composition of deposits. However, it is clearly not a practical technique to deposit functional materials on top of a substrate such as silicon.
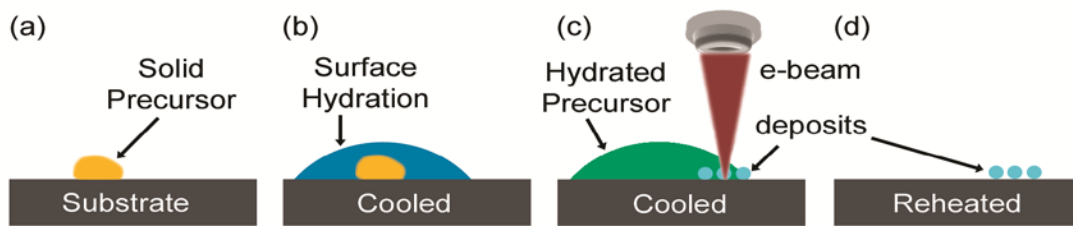
Figure 2-4: Illustration of ex-situ introduction of precursor [17].

A more practical method to perform LP-EBID is to use an Environmental Scanning Electron Microscope (ESEM), where the chamber pressure and sample temperature can be controlled to create an environment that allows liquid precursors to be formed or introduced on a substrate; At the same time, the vacuum would be sufficient to allow a focused electron beam to image and interact with the precursor. Figure (2-4) illustrates a method to form a liquid precursor inside an ESEM chamber. First the precursor is introduced ex-situ using a micro-pipette and left to dry. After inserting the sample inside the ESEM chamber, the sample temperature and chamber pressure are controlled to allow water molecules to condense on the substrate and hydrate the sample. After the precursor is hydrated, a focused e-beam can be utilized to induce deposition of ions that are in the precursor. Finally, the chamber pressure and sample temperature can be modified to evaporate the precursor, leaving behind the deposited structure. As can be seen, this technique allows for direct deposition of materials on a substrate. However, it suffers from a couple drawbacks. First, it is difficult to accurately predict the concentration of the precursor after it is hydrated, which makes this process unrepeatable. Second, ex-situ

introduction of the precursor on the substrate might affect the applicability of such technique in circuit editing since the precursor is not localized to the desired editing spot.
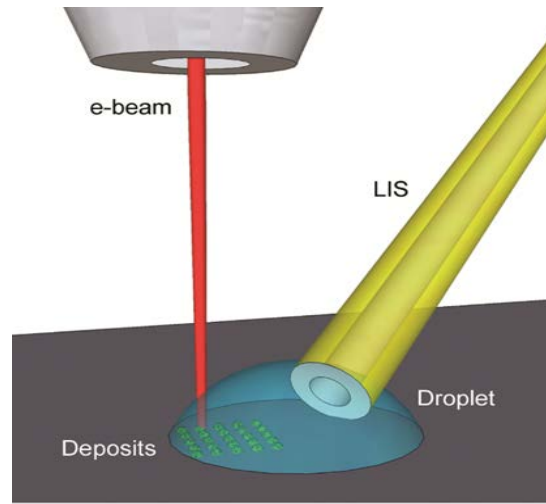
Figure 2-5: Illustration of a Liquid Injection System (LIS). Figure taken from [17].

In [32], a Liquid Injection System (LIS) was developed by FEI for in-situ delivery of liquid precursors inside an ESEM. In the publication, LIS was used to inject a liquid copper precursor on an oxidized silicon Sample to deposit copper inside a controlled vacuum chamber. Illustrated in figure (2-5), the microdroplet, formed by capillary flow of precursor upon touchdown with the substrate, was controlled by adjusting the chamber pressure and sample temperature to offset droplet evaporation rate. This technique provides a solution for a localized delivery of liquid precursors, allowing for true applicability of LP-EBID in circuit edit and device prototype.

2.7 Advantages and limitations of LP-EBID

Several studies show promising results of EBID via liquid precursors in terms of metal content and resistivity (Platinum[14], gold[33], silver[16], and copper[16]) without the need for post processing. Hastings et al. achieved metal content of 70 at. % for copper using LP-EBID with $CuSO_4$ as a precursor[16], which was higher than any other metal content measurement results obtained from conventional EBID of copper. A later study reports copper content of 95 at.% from the same precursor [18]. Furthermore, Hastings et al. demonstrated deposition of silver via LP-EBID, a material that has no gas carrier in EBID. In a separate paper, Hastings et al. shows a ten time increase in LP-EBID

13

deposition rate compared to conventional EBID [14]. The increased material purity, higher deposition rates, and the possibility to deposit new materials provided the motivation for our group to investigate LP-EBID further and to quantify important deposit parameters such as resistivity.

Nevertheless, there are a few challenges to LP-EBID that need to be addressed. One the major challenges is the unwanted collateral deposition and precursor precipitation around deposits. Another challenge in LP-EBID is determining the precursor concentration during deposition. These issues will be discussed in chapter 3.

Chapter 3: Copper – Properties, precursors, and applications

3.1 Importance of Copper

Copper is an important material in the semiconductor industry. Not only is copper an excellent thermal and electrical conductor, but it also has superior electromigration characteristics compared to other metals used in interconnects, such as Aluminum alloys. Electromigration occurs when the momentum of electrons moving in an electric field is transferred to the lattice-bound ions. The result of electromigration is the growth of void areas in the material, which can cause interconnects to break. This issue is exacerbated as ICs, electronic devices, and interconnects get smaller, leading to smaller cross-sectional areas and higher current densities. In a study that compared electromigration resistance between copper and aluminum alloys, it has been shown that copper had a longer lifetime by 1-2 order of magnitude at 275° C and 3-5 order of magnitude at 75° C [34]. Therefore, copper is being considered as an excellent candidate to replace Aluminum alloys as an interconnect material.

In order to deposit copper using EBID, precursor molecules are typically used to carry copper atoms and introduce them inside a vacuum chamber of an SEM, either in a gas or liquid form. Ideally, the precursor will then interact with the focused electron beam, which should dissociate the copper atoms from the precursor molecules and deposit copper onto a substrate. The purpose of this chapter is to provide a brief literature review on previously used copper precursors.

3.1 Copper precursors in EBID

Most of the gaseous precursors used in EBID have been inherited from Chemical Vapor Deposition (CVD). CVD is a deposition method involving the application of heat to induce film deposition of materials from gaseous precursors in inert gas environments. Many of these precursors are organic in nature, where the desired material is bonded to complex carbon-oxygen-hydrogen rings, and have relatively low vapor pressures at room temperature. The low vapor pressure means that the precursors are stable enough to be introduced to a high vacuum chamber, assuming the chamber is at room temperature. However, for EBID, the precursor molecules also need to be easily dissociated by an electron beam (separating the desired material from its carrier gas), which requires the

precursors to have a certain degree of chemical instability [27]. Although many of these precursors were successfully used in EBID, several issues arose throughout the years as they were not fully optimized for EBID use. Unfortunately, with regard to EBID of copper, there is not a perfect gaseous precursor from which copper can cleanly dissociate, and therefore, as can be verified by the literature, the deposited copper usually incorporates varying degrees of precursor elements.

The most common copper precursors used in the literature include the following:

- Cu(II)(hfac)$_2$ – *hfac: hexafluoroacetylacetonate*
- (hfac)Cu(I)(MHY) – *MHY:2-methyl-1-hexen-3-yne*
- (hfac)Cu(I)(VTMS) – *VTMS: vinyltrimethylsilane*
- (hfac)Cu(I)(DMB) – *DMB: dimethylbutene*.

The discussion following will be limited to metal content and resistivity:

Ochiai et al. used (hfac)Cu(I)(VTMS) to study the deposition rate, composition, and resistivity of the deposited copper [35]. The authors report resistivity of copper at 3.6 $\mu\Omega \bullet cm$, with Cu metal content of 11 at. %. Notice that the resistivity reported is very close to bulk copper resistivity of $\sim 1.6\ \mu\Omega cm$. In his review of EBID precursors, Botman et al. mentions this discrepancy in the resistivity results of copper, with the conclusion that the results of [35] were never repeated, but rather contradicted with the findings of [25], which showed insulating behavior for copper deposits.

As far as the metal content and composition of the deposited copper, most reviews and studies agree that the use of the mentioned precursors yields copper nanocrystals embedded in a carbonaceous matrix, with copper content not exceeding 12 at.% [11-13, 24, 27, 36]. The exception is in [25] where copper deposits from low stability precursors (hfac)Cu(I)(VTMS) and (hfac)Cu(I)(DMB) were found to be 45-60 at. %. Also, Miyazoe et al. used H$_2$/Ar micro-plasma-assisted EBID and achieved a 41 at.% for copper deposits from Cu(II)(hfac)$_2$ [37]. Finally, Thompson et al. used a hydrogen/oxygen post-treatment of the deposit and achieved an 99 at.% for copper deposits from (hfac)Cu(I)(VTMS) [38]. However, total hydrogen/oxygen exposure time exceeded 40 hours.

A recent comparative study on the resistivity of EBID of copper deposits from $Cu(II)(hfac)_2$, $(hfac)Cu(I)(VTMS)$, and $(hfac)Cu(I)(DMB)$ suggest insulating behavior of the copper nanowires[11, 12]. The study investigated the effect of hot plate, laser pulse, and TEM (Transmission Electron Microscope) annealing on the properties of the copper deposits and nanowires. The as-deposited copper from $Cu(II)(hfac)_2$ amounted to 10 ± 2 at.% that was embedded in a carbonaceous matrix. Copper content from $(hfac)Cu(I)(VTMS)$, and $(hfac)Cu(I)(DMB)$ was twice as high. Annealing the copper deposits did not change the metal content significantly and caused a 70% decrease in volume of the deposits due to the reticulation of the carbon network after the release of fluorine and oxygen from the deposit. The recorded resistivity of the as-deposited copper nanowires was ~10 kΩ•cm, which was reduced to ~1 Ω•cm after annealing. Figure (3-1a) below is a micrograph of the deposited nanowire, where crystallization of copper is visible after annealing processes in figure (3-1b). Figure (3-1c) provides a close up image of the copper nanocrystals embedded in the carbonaceous deposit. Figure (3-2) shows a plot of the resistivity vs. temperature for a nanowire deposited from $Cu(II)(hfac)_2$ which reflects the high resistivity, even after annealing, of the nanowire. The inset micrographs in figure (3-2) show the effect of temperature on the morphology of the wires. Aside from the expensive cost of the above precursors, the poor purity content and high resistivity from EBID of these precursors impede the use of copper in practical EBID applications.
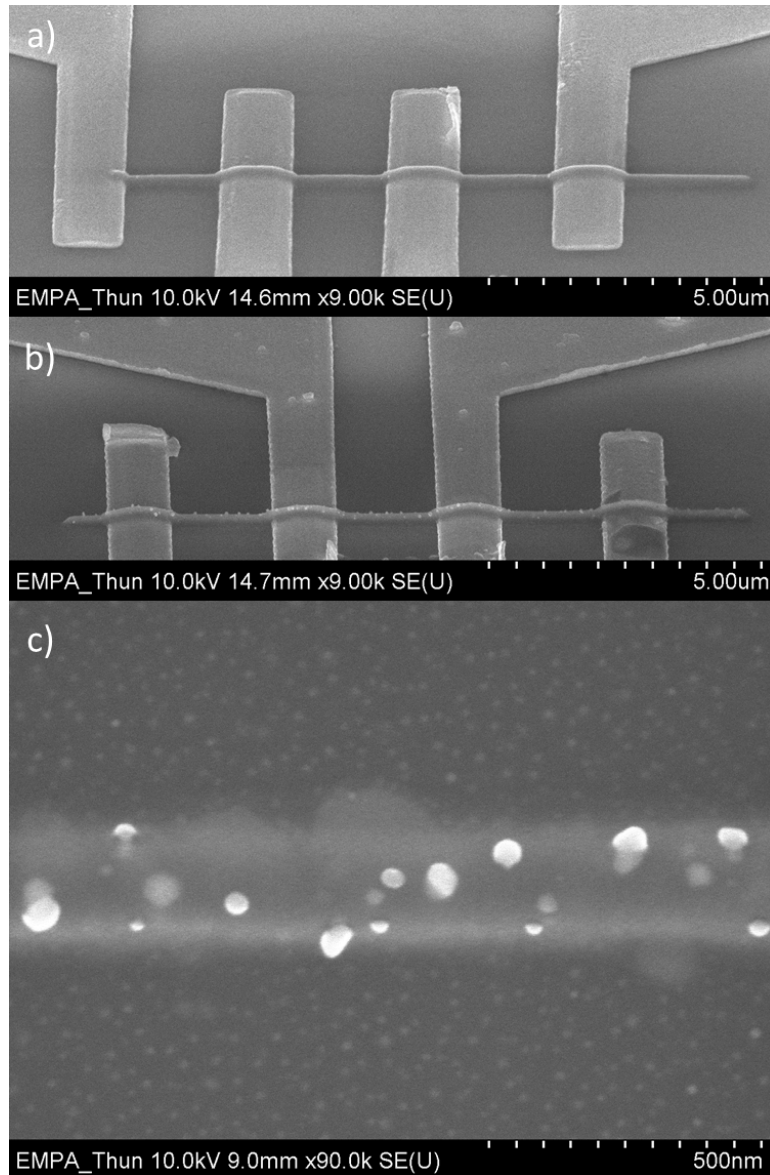
Figure 3-1:Figure taken from [11] a) As-deposited nanowire from $Cu(II)(hfac)_2$ via EBID connecting a gold four point pattern circuit. b) Crystallization of copper after annealing attempt is visible on the nanowire. c) Close up snapshot of copper nanocrystals in the nanowire.
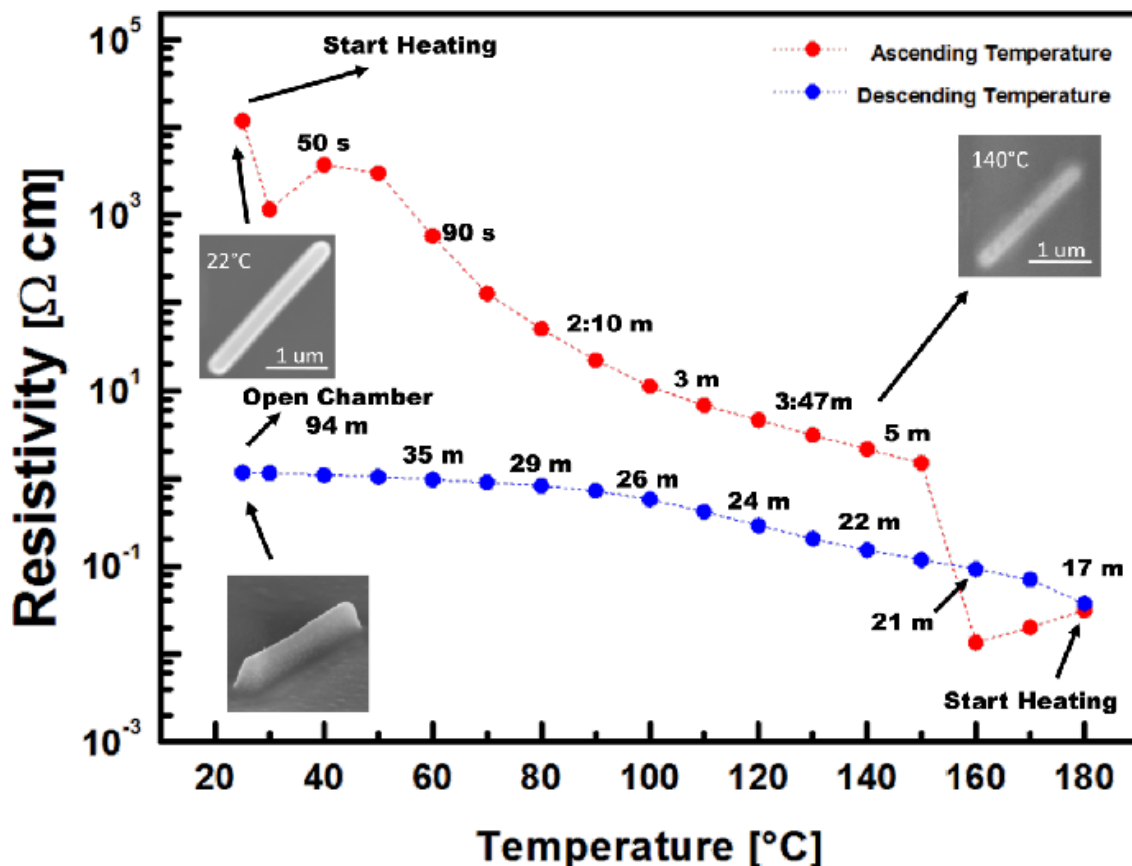
Figure 3-2: Plot of resistivity of nanowire deposited from Cu(II)(hfac)$_2$ vs. temperature [11, 12]. Insets: Temperature induced morphology changes in nanowire.

3.3 Copper precursors in LP-EBID

In 2013, Botman et al. demonstrated LP-EBID of copper from a copper sulfate solution (CuSO$_4$) using a liquid injection system (LIS) in an ESEM. The study explored a technique of stabilizing a precursor droplet in a controlled temperature and pressure environment, as well as demonstrated deposition on conductive and insulating substrates. A low concentration of the precursor, 0.8 mM CuSO$_4$, was used in order to avoid salt crystal formation that would block the LIS. Through Energy Dispersive Spectroscopy (EDS) analysis, the authors concluded that high purity copper was deposited, although no specific metal content data was provided. However, precipitation of residual salt contaminants was also observed. In addition, the study highlights important precursor wetting dynamics. Due to surface tension forces, the precursor microdroplet naturally forms a steep bow-shape thick edge with the surface of the substrate, as shown in figure

19

(3-3). A thick droplet profile can reduce pattern fidelity and repeatability, as well as change the path of the e-beam, which affects patterning precision [16]. These issues are detrimental to the patterning of interconnects. In order to circumvent this issue, the authors found that applying a small bias between the precursor droplet and the conductive metal substrate can affect the wetting process through a phenomenon called electrowetting. By applying a bias, the contact angle of the microdroplet with the substrate (wetting ability) can be modified to form a thin droplet edge profile. In the case of insulating substrates, wetting of the precursor can be modified by introducing subsurface charging of the substrate.
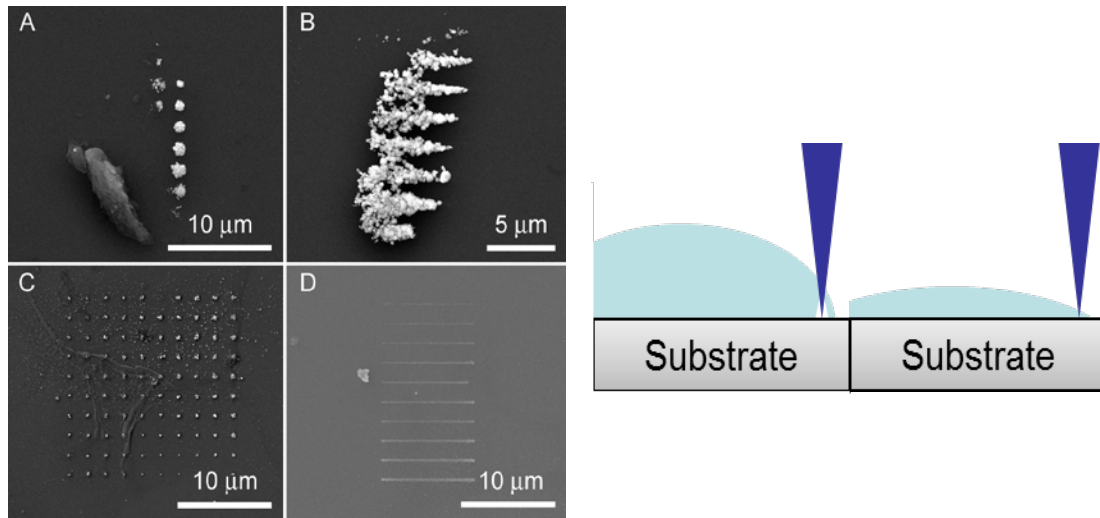
Figure 3-3: Illustration of droplet edge thickness and its effect on the deposit profile [16].

Hastings et al. also demonstrated LP-EBID of copper from the same precursor, $CuSO_4$, using an ESEM. Two methodologies were used to deliver the precursor: in-situ hydration of solid precursor and in-situ injection of liquid precursor. For the former method, the precursor concentration was between 100-500 mM. The latter method diluted the concentration of $CuSO_4$ to 300 µM in order to avoid blockage of the LIS. The authors report copper content of 70 at.%, an unprecedented result in the literature of EBID at the time. The main contaminants were carbon (~13 at.%) and oxygen (16 at.%). Some salt precipitation was noticed and was treated with a DI H_2O wash after deposition. Similar to [32], achieving a thin liquid layer for deposition was challenging. The authors were able to alleviate this issue by adding a surfactant agent, sodium dodecyl sulfate (SDS), to the

precursor mix. Adding the surfactant agent helps relax the surface tension forces and reduce the contact angle of the droplet with the surface of the sample. The result was enhanced pattern fidelity and repeatability. Using an optimized precursor mix of 0.25 M $CuSO_4$ + 4 mM SDS, the authors report line resolution of 70 nm, with dots as small as 100 nm in diameter. These deposits showed no increase in carbon contamination compared to a bare substrate, however, subsequent experiments revealed carbon contamination [18]. Finally, the paper presents two possible deposition mechanisms in liquid precursors – electrochemistry and radiolysis. The reduction of copper (II) ions to copper metal during LP-EBID is realized either with radiation chemistry, electrochemistry, or a combination of both. With radiation chemistry, the secondary electrons interact with water molecules to become solvated electrons, which then reduce copper ions to copper metal inside the solution. On the other hand, electrochemistry suggests that the electron beam acts as a virtual cathode on the substrate, reducing copper ions and depositing copper on the substrate through directly transferring electrons in the reduction process. The paper calls for further research to investigate which mechanism dominates during the deposition process.

The effect of utilizing a thin precursor film for deposition was further highlighted in [39]. The study used a liquid sample holder to control the liquid film of $CuSO_4$ precursor inside a TEM up to an estimated thickness of 210 nm. Copper patterns finer than 100 nm were produced. The authors conclude that pattern fidelity could be enhanced by further reducing the liquid film thickness and using smaller e-beam convergent size.

Den Heijer et al. provided further insight on the mechanisms behind the growth of nanostructure from copper precursors. In this case, the precursor was 0.1M $CuSO_4$ + 0.18M H_2SO_4 + 1.4mM HCL, which was placed in an electrochemical cell and inserted into a TEM. The deposition was performed via standard electrochemical deposition using a gold electrode, and the electron beam was allowed to scan the cell. The authors report that the effect of the electron beam on the growth of the nanostructures is dependent on the electrolyte chemistry. By adding chloride ions, they were able to use the e-beam to enhance the nucleation of copper clusters. The authors conclude that electrochemistry is

21

not the only governing deposition mechanism, and that radiation chemistry plays an important role in deposition from liquid precursors [31].

Recently, our group performed a study that focused on improving the purity content, resolution and fidelity of LP-EBID of copper. The paper identifies additives such as SDS, Triton X-100, Polyethylen glycol (PEG), sulfuric acid (H_2SO_4), and bis-(3-sulfopropyl) disulfide (SPS) that could be incorporated with $CuSO_4$ to enhance the conditions of deposition and the deposit characteristics by exploiting the chemical benefits of each additive. SDS, a common surfactant agent, was found to increase pattern resolution by thinning the precursor droplet edge and minimizing beam scatter in the electrolyte. Triton X-100, a nonionic surfactant, was found to help reduce surfactant precipitate, which was an issue with SDS. However, caution must be exercised with using Triton at high concentrations, as it tends to form an insoluble gel that precipitates on the substrate. Sulfuric acid (H_2SO_4) improves the stability of the precursor droplet inside the ESEM due to its low vapor pressure, and works to lower the contact angle of the precursor droplet and the oxygen contamination in the deposits. Moreover, the presence of H_2SO_4 in the precursor helps in estimating the concentration of the precursor after hydration in the ESEM [40]. PEG and SPS are usually used in electroplating. PEG acts as a suppresser that inhibits deposition, a property that was exploited to reduce unwanted copper deposition, while SPS acts as an anti-suppressor that promotes deposition, allowing for finer grained deposits. The results of the study report a copper purity of 95 at.% from $CuSO_4$. Furthermore, additives were found to reduce the purity. However, the lowest reported purity was with using $CuSO_4$ + PEG, which yielded ~87 at.% This is still a significant improvement over gas-phase EBID of copper. Although the addition of PEG reduced the purity of the deposits, it was found to increase pattern fidelity. The results also show that the highest resolution patterns were achieved with $CuSO_4+H_2SO_4+$Triton X-100 (100 nm pitch nested lines). Finally, the study concludes that there is significant evidence that radiolysis plays an important role in the deposition process along with electrodeposition, emphasizing the complexity of LP-EBID. The high purity content of copper achieved via LP-EBID provided the motivation for this study to quantify the resistivity of LP-EBID copper nanowires. Furthermore, up to this work, there are no reports on the resistivity of copper deposited via LP-EBID.

Chapter 4: Experimental Process

In this chapter, I will present and discuss the process for preparation, deposition, and resistivity measurement of copper nanowires using the LP-EBID technique. Since the goal of this work is to quantify the resistivity of the copper nanowires, a brief discussion of the measurement methods is warranted. A four point measurement technique is used to measure the resistance of the nanowire. Figure (4-1) illustrates this technique. The benefit of the four point measurement technique is that it minimizing the effect of contact resistance of the probes, leading to more accurate measurements. In order to use the four point measurement technique, a four point pattern is needed. A discussion on fabricating the four point pattern will be presented in section 4.2.
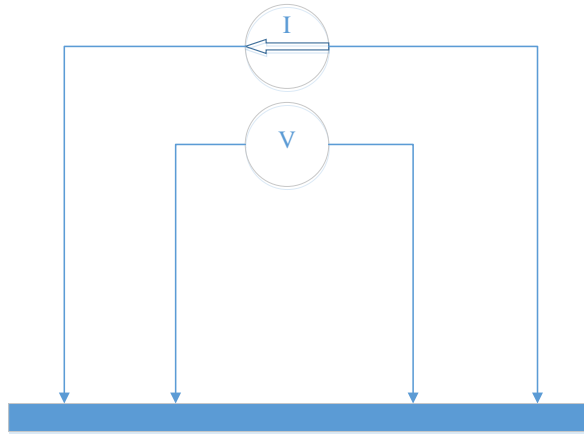
Figure 4-1: Illustration of four point measurement technique on a wire. The outer leads source current, wheras the inner leads measure the voltage.

This chapter will first present the starting materials for the experiment, mainly the type of wafer used and the copper precursor. Then, a detailed description of the sample preparation steps will follow, which involves using the process of electron beam lithography (EBL) to develop four point patterns that will assist in measuring the resistivity of the nanowires. After that, I will discuss the methods and conditions used in depositing the copper nanowires. Finally, I will present the process behind obtaining the resistivity data. Figure (4-2) illustrates the sequential steps for the entire experiment.
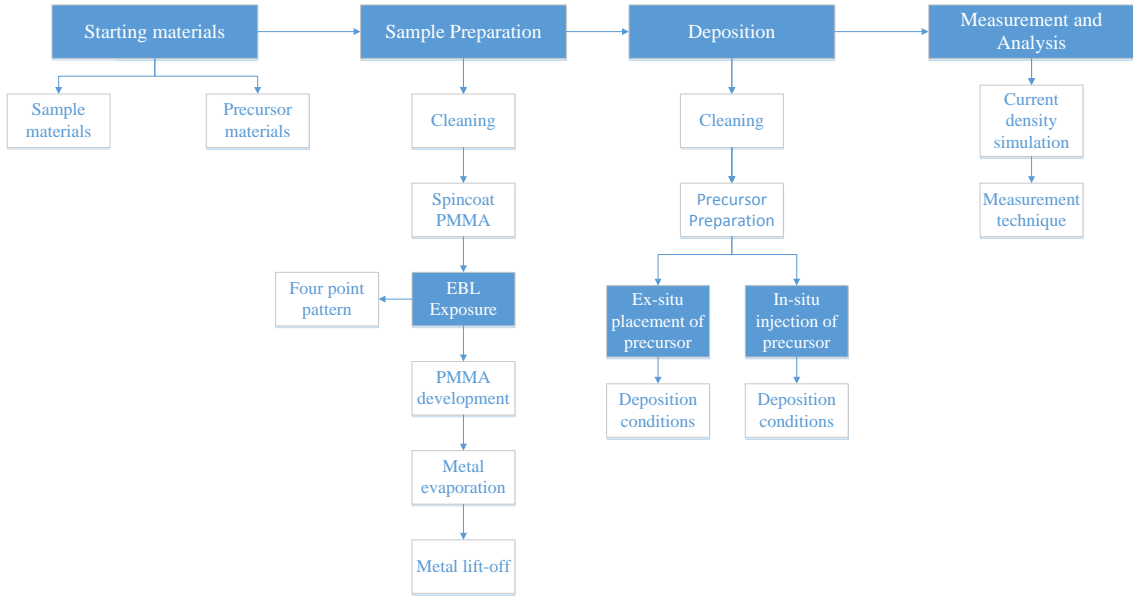
Figure 4-2: experimental process for extracting the resistivity of a copper nanowire deposited via LP-EBID.

4.1 Starting materials and equipment

Throughout the entire experiment, a silicon wafer with thick oxide layer (1.7 µm SiO$_2$) was used. The thick oxide layer serves as a good insulator to reduce the leakage current into the wafer as the resistance of the nanowire is measured.

The precursor solutions contained two main components, diluted Copper Sulfate CuSO$_4$.5H$_2$O (Fisher Scientific) in deionized water (DI H$_2$O) and Sulfuric acid, H$_2$SO$_4$ (EMD Millipore). Copper deposition from copper sulfate solution has been mentioned in chapter 3. In addition, copper deposition from sulfuric acid has been noticed before, where focused electron-beam induced etching of copper film using sulfuric acid showed redeposition of copper after the etching process [41]. Also, as mentioned before, it is convenient to use sulfuric acid for its low vapor pressure [40] and Control/estimate concentration based on equilibrium with water vapor. Additives such as sodium dodecyl sulfate – SDS (Acros Organics), Triton X-100 (Sigma-Aldrich) and polyethylene glycol with a molecular weight of 1000 – PEG 1000 (VWR), were added where specified to improve wetting of precursor during the experiment and provide finer grained deposits. I will reference these additives, along with molar ratios and concentrations, with the results of nanowire deposits in chapter 5.

24

4.2 Sample preparation

As mentioned, a four point pattern is essential to perform resistivity measurements on the nanowires. Figure (4-3) shows two examples of four point patterns. The idea is to provide large enough pads for a four point meter to connect to the nanowire which will be deposited at the terminal ends of the large rectangular pads, effectively closing the circuit. The pads are 100x100 µm, and the terminals extending from the pad are 1 µm wide. This section covers the process behind obtaining these structures and making them electrically conductive.
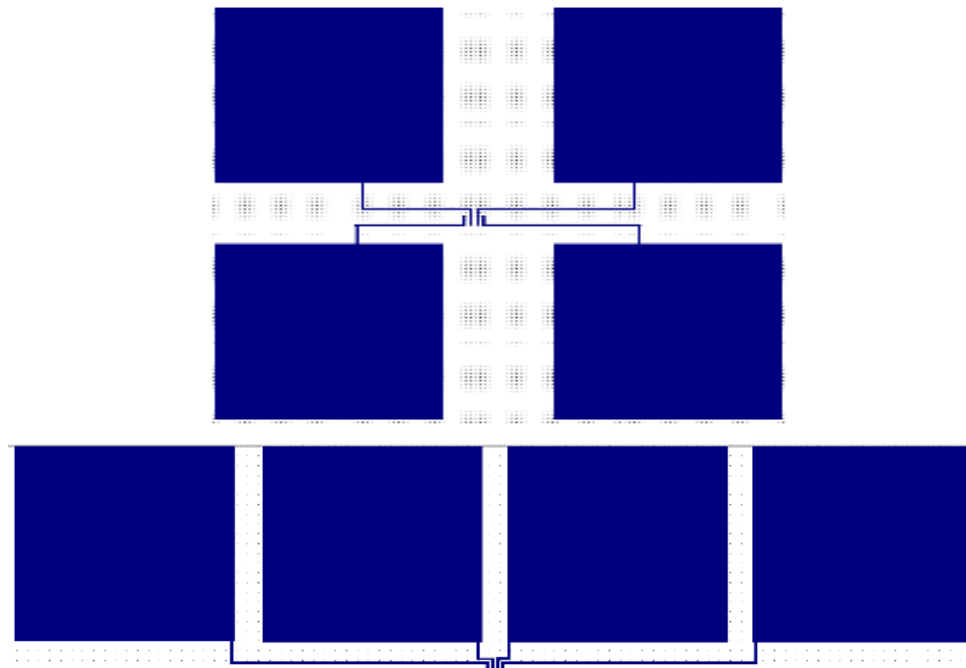
Figure 4-3: Examples of four point structures that are used to measure the resistance of nanowires. A Copper nanowire must be deposited via LP-EBID where the probe terminal wires align in the middle. Top, or inner, squares measure voltage. Bottom, or outer, squares source current.

The sample preparation procedure consists of the following steps which are also illustrated in figure (4-4):

1. Start with a silicon wafer with thick oxide layer

2. Sample cleaning/Spincoat PMMA resist

3. EBL exposure and PMMA development

4. Cr/Au evaporation

5. Metal lift off
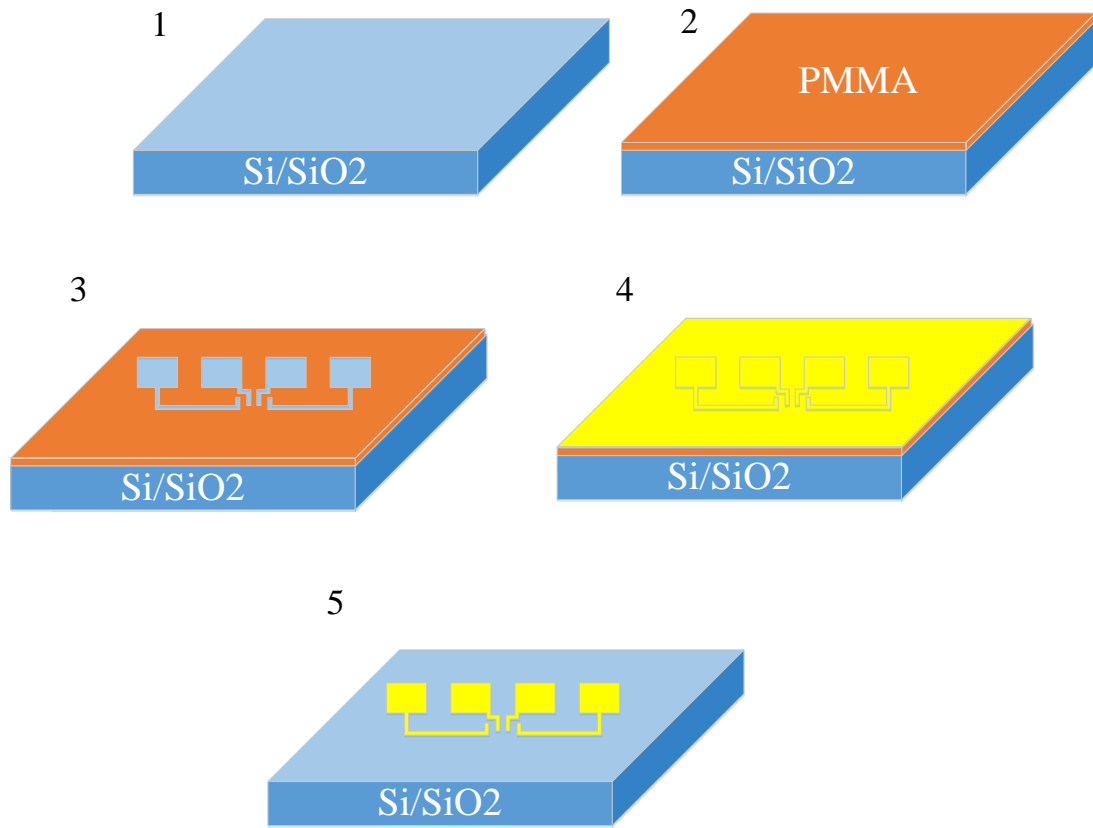
Figure 4-4: Illustration of sample preparation procedure.

4.2.1 Setting up for e-beam lithography

This process takes place in a class 10/100 cleanroom. The samples are first washed with Aceton (Fisher Scientific), Isopropanol (IPA, Fisher Scientific), and DI water for 15-20 seconds each. A spincoater is used to apply a uniform layer of photoresist on top of the sample. The thickness of the photoresist is a function of the rpm of the spincoater. In all experiments, 950PMMA A2 (Microchem) was used (950 refers to the molecular weight, A2 refers to 2% dilution by anisole. Hence, 98% of the weight is Anisol). Typically, a pipette is used to cover three quarters of a sample with PMMA before spincoating. The PMMA layer typically needs to be at least 3 times as thick as the final structure thickness.

Since the final four point structure is expected to be ~35 nm thick, the thickness of the PMMA needs to be at least > 105 nm. After consulting the PMMA datasheet from Microchem, the spincoater spin speed was set to 1100 rpm, which should result in ~150 nm thick PMMA, which is enough for the purpose of this work. After spincoating the sample with PMMA, a hot plate was used to perform a soft back at a 180° C for a minute on the sample in order to remove the solvent (anisole) and make the unexposed PMMA less soluble. An ellipsometer is used to verify the thickness of the PMMA layer. Ellipsometery is an optical technique that can be used to measure the thickness of sample layers by analyzing the change in light polarization after reflecting off of the material. Figure (4-5) shows the setup for an ellipsometer.
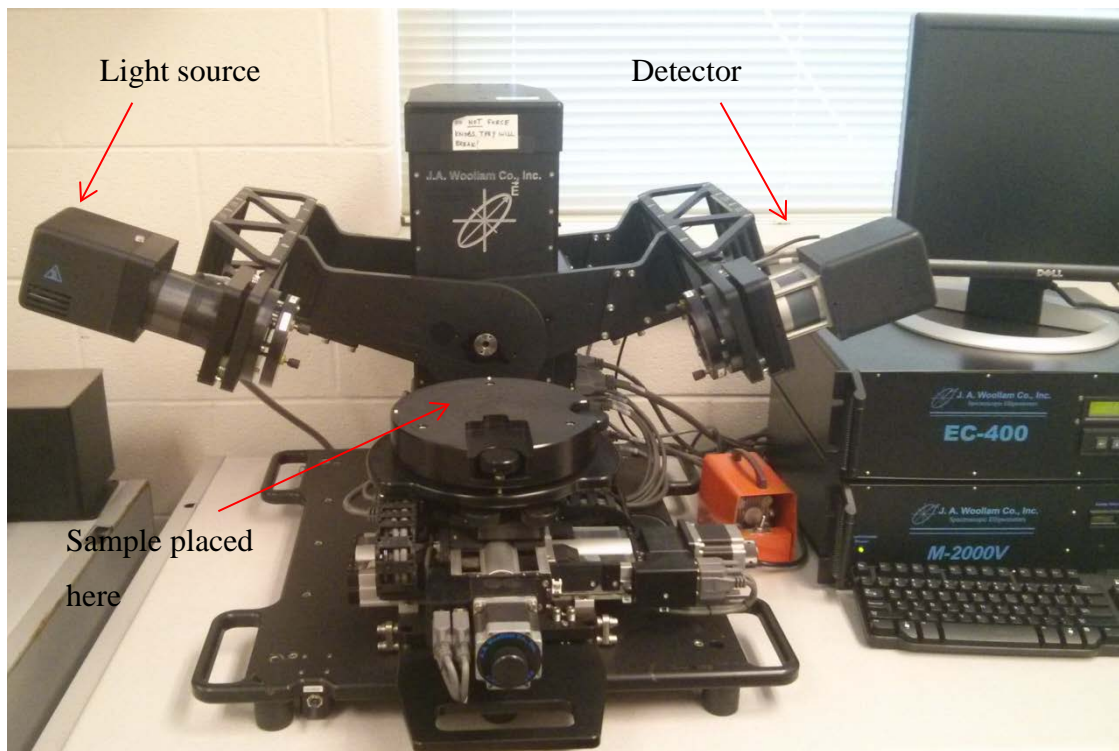
Figure 4-5: Setup for ellipsometer. Light from the source passes through a polarize, reflects off of the sample and is analyzed by the detector to determine film thickness.

4.2.2 EBL exposure and development of photoresist

Electron beam lithography works by taking advantage of the irradiation of electrons to cross link or break polymer chains in photoresist materials. Negative photoresists cross link (become rigid) after e-beam irradiation, whereas positive photoresists break down upon electron irradiation. PMMA is a positive photoresist. The EBL used in this experiment is a Raith E-line. Unlike photolithography, Electron beam lithography is a maskless lithography technique. The Raith e-line is equipped with CAD software that enables the design of patterns to be transferred to the sample. In the case of this experiment, a matrix of four point patterns was drawn on the cad software. The exposure conditions were 10 kV with area dose of 110 µC/cm^2. Different aperture sizes were used between different samples (30 µm-60 µm). The aperture size affects the current of the beam. Higher currents reduce exposure time at the cost of resolution.

After the pattern has been transferred onto the photoresist-coated sample, it is treated with a photoresist developer in order to remove the exposed (soluble) photoresist. The developer used in this experiment is MIBK-IPA 1:3 (Microchem). This leaves the sample ready for metal evaporation.

4.2.3 Evaporation and metal lift-off

An electron beam evaporator (Kurt J Lesker), was used to evaporate an adhesion layer, titanium, and gold onto the sample. Electron beam evaporation works by heating metal pallets using a high energy electron beam. Once atoms gain sufficient energy to separate from the surface of the metal, they traverse the vacuum chamber to be deposited on a sample. The process is performed under vacuum to minimize the collision of source atoms with air molecules.

The end goal behind metal evaporation is to fill in the four point probe pattern with a layer of gold. However, an adhesion layer is required between SiO_2 and gold. The most commonly used adhesion layers are chromium, nickle, and titanium. Typically, the adhesion layers needs to be only a few nanometers thick (> 2 nm). In this case, Titanium and chromium were used interchangeably between samples with a thickness aim of 5 nm, whereas gold was deposited at a thickness of ~30 nm.

The e-beam evaporator was allowed to pump down for 3-4 hours to achieve high vacuum (10^{-7} torr), the evaporator is multi target, which means that titanium and gold can be deposited without breaking vacuum (important to avoid oxidation of titanium and create surface non-uniformity by having unwanted air molecules stick to sample surface between Ti and Au layers). Also, the evaporator contains a water cooling system to avoid heating of the sample and damaging the PMMA. Once the pressure reached 10^{-7}, deposition of titanium was initiated. A quartz crystal was used to measure the thickness and the rate of film growth. Once the Ti reached 5 nm, it was switched to gold and deposition was initiated. A 30 nm of gold was deposited making the total structure thickness 35 nm, well below a third of the photoresist thickness.

Up to this point in the sample preparation process, the entire sample is covered in Cr/Au. Metal lift off uses a solvent that attacks and removes the photoresist from the substrate, leaving behind the coated patterns. In this experiment, N-Methyl-2-pyrrolidone (NMP, Fisher Scientific) was used for metal lift off process. The sample was submerged in NMP at 60° C until the Cr/Au layer is seen as peeling off from the sample except around the four point pattern. If all of the Cr/Au is not peeled away, shaking the beaker might help. If that doesn't work, then sonication can be used to aggressively remove the rest of the Cr/Au. Caution: sonication can destroy parts of the four point pattern, so check the sample frequently. The sample is now ready for an LP-EBID of copper nanowire experiment.

4.3 Deposition Process and Conditions

All depositions were carried out in a Quanta 250 FEG (FEI Co., Hillsboro, OR, USA), shown in figure (4-7), operating in ESEM mode equipped with a Raith Elphy 7 electron beam lithography pattern generator system. ESEM permits deposition on bulk substrates without the use of liquid cells [16]. Gaseous secondary electron detector (GSED) was needed for low vacuum imaging. Prior to any experiment, the samples were rinsed with IPA, and DI water for 20 seconds each. In addition, plasma cleaning was conducted on all samples to remove organic contaminants, which helps reduce contaminants in the deposit, and make the surface of the sample more hydrophilic. All deposition processes were conducted using 30 kV accelerating voltage, and sample temperature of 3°C –

cooling was provided by placing sample on a peltier stage and applying silver paste to thermally connect the top of the sample with the base of the stage. Beam current was measured using a faraday cup and a Keithly 6487 picoammeter. Reports of beam currents and dose will accompany the results of the nanowire deposits later in this paper.

Delivery of precursor on the substrate was achieved through two techniques: ex-situ delivery or in-situ injection. Ex-situ delivery of precursor involved using a micropipette and an optical microscope in order to place the precursor close to our four pad structures. After the precursor was left to dry, the system was pumped down to 5.5 torr. Condensation on the sample surface was then controlled by increasing the pressure slowly, while keeping the sample at ~ 3°C, until the copper crystals dissolve and a stable precursor droplet is achieved. The challenging part with this set up is to get the droplet edge close to where the nanowire is to be deposited, where the only viable means of controlling the liquid edge movement is to vary the pressure (hydrating/dehydrating) inside the chamber. Not only is this a challenge, but it also eliminates repeatability of the experiment, since exact concentrations of copper in the liquid cannot be determined from experiment to experiment. After driving the liquid edge to the deposition area and stabilizing the droplet, the pattern generator can be used to focus the electron beam on the edge of the droplet to deposit the wire.

Alternatively, a liquid injection system (LIS) developed by FEI [32] could be used to inject the precursor in-situ. The LIS employs a nanocapillary (NC) needle made from borosilicate material and formed using standard pulling technique. The diameter of the NCs were 2-6 µm. Using LIS, the precursor delivery on the substrate becomes more localized, eliminating the need to drive the liquid edge by varying the pressure of the chamber. This adds more certainty to concentration estimates of copper ions in the precursor solution during the deposition process. Figure (4-6) shows a micrograph of the nanocapillary needle placing a precursor microdroplet near a four point pattern. The flow of precursor was initiated upon touchdown with the sample, and the size of the droplet was controlled by varying the pressure of the chamber.

After the nanowire has been deposited, the chamber is vented and the stage is restored to room temperature. Using a micro-pipette, a small droplet of DI water is placed on the

sample and then washed away to treat salt residue from the precursor. The sample is then put back into the chamber and imaged in high vacuum mode in order to measure the nanowire dimensions.
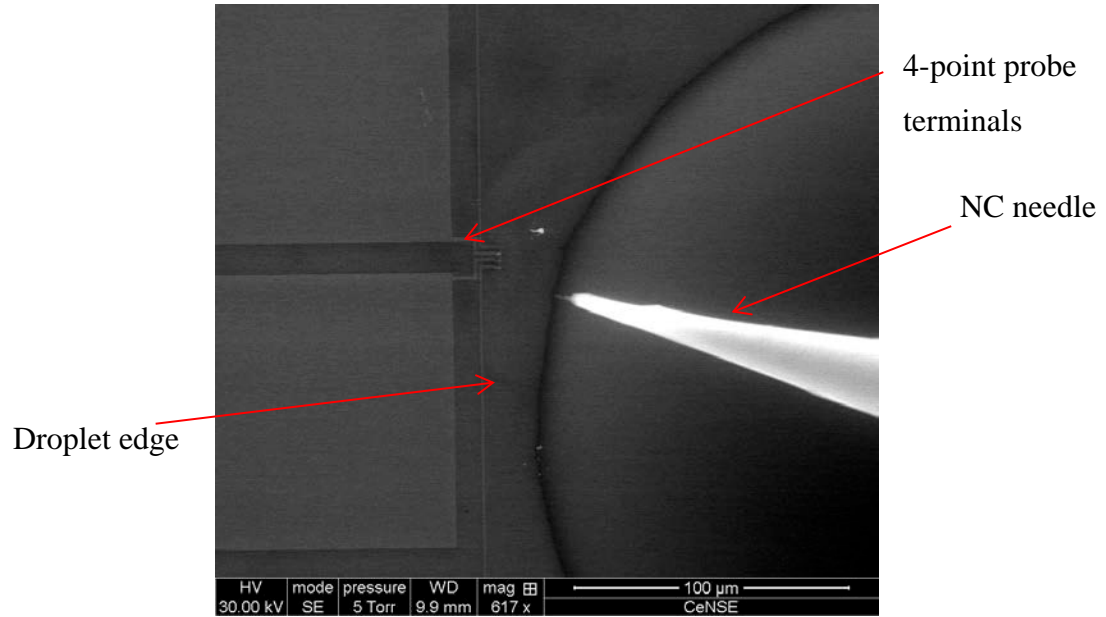
Figure 4-6: Micrograph showing an NC needle forming a microdroplet near a gold four point pattern.

Figure 4-7: An Environmental Scanning Electron Microscope (ESEM) supplied by FEI.

4.4 Extraction of resistivity

Electrical resistivity is a material property that quantifies the materials response to an electric current. As electrons in metals respond to an applied electric field, they start hitting other atoms in the lattice as they drift, transferring some of their energy to the atoms in the form of heat. For wires, this phenomenon can be quantified by the equation (4-1). The resistivity of the wire is dependent on the wire's dimensions and measured resistance.

$$\rho = \frac{R \times A}{L} \; [\Omega \cdot m] --- (1)$$

In addition, current density can be a critical factor in nanowires. For such small features, it is easy to reach current densities that cause the wire to break due to electromigration or melt. According to [42], copper nanowires withstood current densities of 10^8 A/cm^2. In order to get a metric for how much current the copper nanowire can support, a current density simulation, shown in figure (4-8), was performed for a copper nanowire and gold electrodes sourcing 1 mA of current. The wire is 10 µm long, 0.5 µm wide, and 0.6 µm high, which is close to the dimensions of deposited copper wires that will be reported in chapter 5. As can be seen from the simulated wire, the current density peaks at ~ 5.2457×10^6 A/cm^2, well below the 10^8 A/cm^2 limit, and is uniform across the wire. It is interesting to see how the current density tends to peak at the edge of the terminals, illustrating how current tends to seek the shortest (less resistive) path.
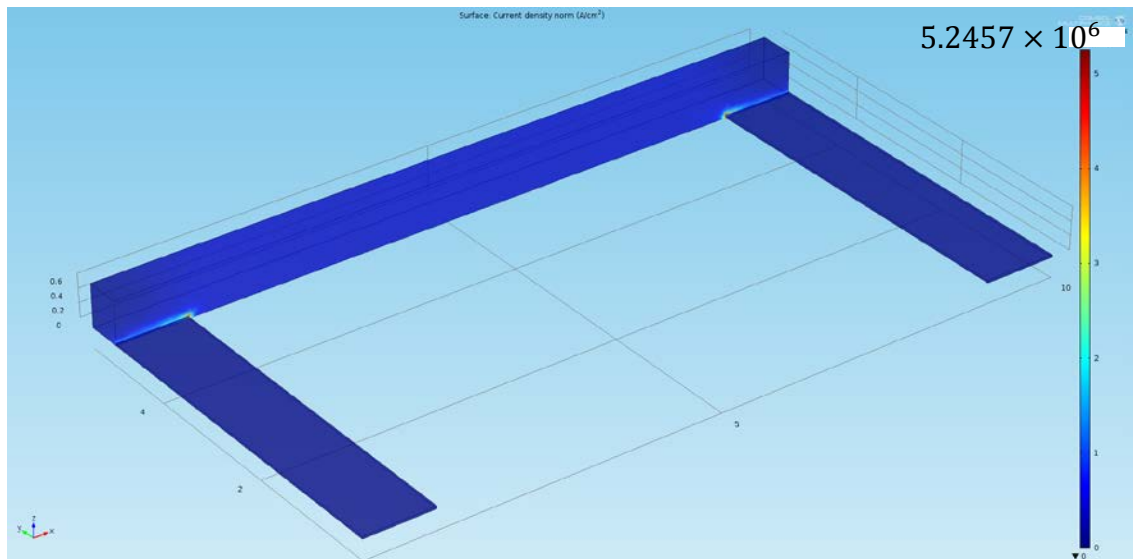
Figure 4-8: Current density simulation for a copper nanowire. COMSOL 4.2 was used as the simulation software package.

Measurement of nanowire resistance was performed using a four point probe station, supplied by Cascade Microtech, shown in figure (4-9), which was connected to a keithley 6430 meter with three axis moving stage and tungsten leads. Caution should be used when leads touchdown on the four point pattern, as they can scratch away the gold coating or break the terminals. The keithley meter is controlled by a MATLAB code (supplied in the appendix) through a GPIO connector. The meter performs a linear sweep

over a defined current range and measures the voltage, and then MATLAB reads the measured values and calculates the resistance of the nanowire by finding the slope of the linear sweep. Equation (4-1) is then used to extract the resistivity using the wire's dimensions and measured resistance.
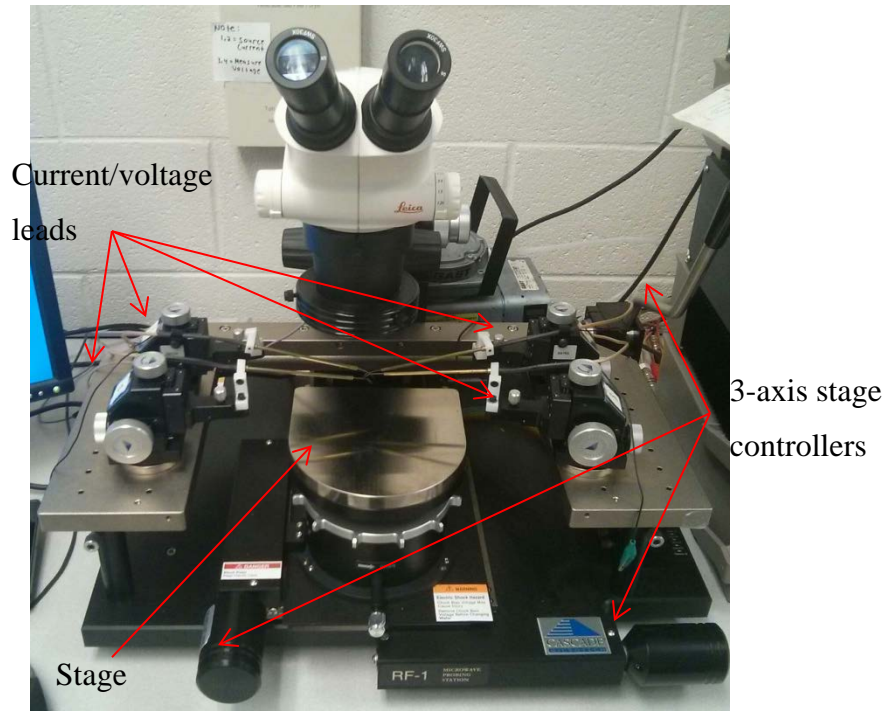
Figure 4-9: Setup of a four point probe station. The leads end with tungsten needles with 2-12 µm tip.

Chapter 5: Discussion of Results

Up till this work, there have been no reported measurements of resistivity for LP-EBID deposits for copper. The experimental process for this thesis was started by a fellow colleague, Adham Noubani, where initial results of resistivity quantification were obtained from a copper nanowire, shown in figure (5-1), that was deposited from the precursor $CuSO_4.5H_2O$ + SDS using the ex-situ precursor placement technique [43]. The obtained resistivity was 1.84 μΩ•cm, a remarkably close value to bulk copper resistivity of 1.68 μΩ•cm. However, significant salt deposit and collateral deposition is visible around the wire. This chapter will highlight recent resistivity results from LP-EBID of copper nanowires and analyze the results in comparison to previous works in EBID. This chapter will also present the challenges associated with deposition, such as salt deposit and collateral deposition, and provide some insight on possible solutions.
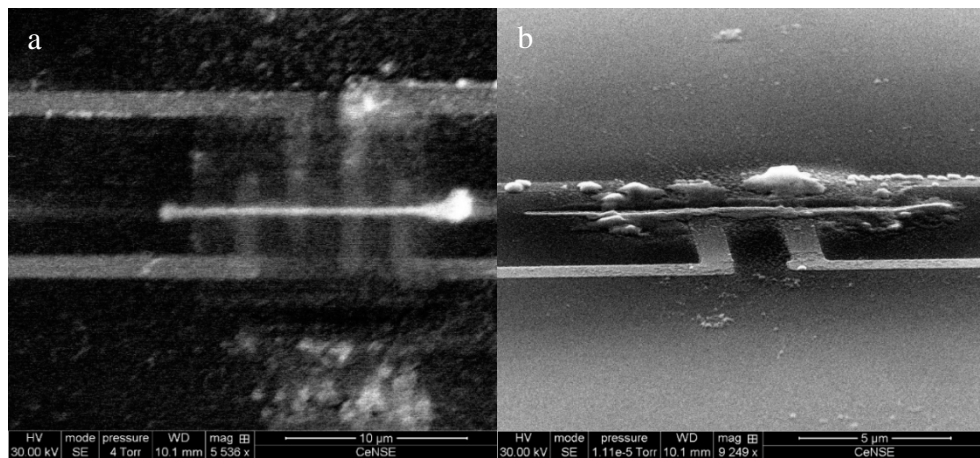
Figure 5-1: Initial LP-EBID of copper nanowire by Adham Noubani. (a) Top view of copper nanowire deposited on gold four point pattern. (b) 60° tilt view of copper nanowire in (a) [43]

5.1 Results and analysis

Figure (5-2) and table (5-1) below show four successful depositions for copper nanowires along with specific deposition conditions and wire dimensions using different additives with $CuSO_4+H_2SO_4$. The best resistivity achieved was 67 μΩ•cm, correlating to figure (5-2d), with 0.25M $CuSO_4$+ 0.1M H_2SO_4+ 8mM SDS using the LIS. The same precursor was used under different deposition conditions which yielded a resistivity of 370 μΩ•cm,

correlating to figure (5-2c). SDS was mainly used to reduce the contact angle of the microdroplet to improve pattern fidelity.

PEG and Triton X-100 were also used in successful nanowire depositions. Figure (5-2a) shows deposited nanowire from 0.25M $CuSO_4$+ 0.1M H_2SO_4+ 100ppm PEG 1000 where the extracted resistivity was 5000 $\mu\Omega\bullet$cm (Note that before FIB milling, the resistivity was 3500 $\mu\Omega\bullet$cm). PEG was mainly used to inhibit the deposition of copper in an attempt to reduce unwanted copper deposition. Figure (5-2b) corresponds to deposition from 0.25M $CuSO_4$+ 0.1M H_2SO_4+ 1mM Triton X-100 with extracted resistivity of 800 $\mu\Omega\bullet$cm. Triton was used as a nonionic surfactant in an attempt to reduce the precursor precipitate as well as provide a thin liquid edge for finer depositions. The constant patterning conditions across all depositions were the sample temperature, $3°$ C, and beam accelerating voltage, 30 kV. The rest of the patterning conditions are reported in table (5-1). No post-processing steps, such as thermal or e-beam annealing, were performed on any of the deposits.
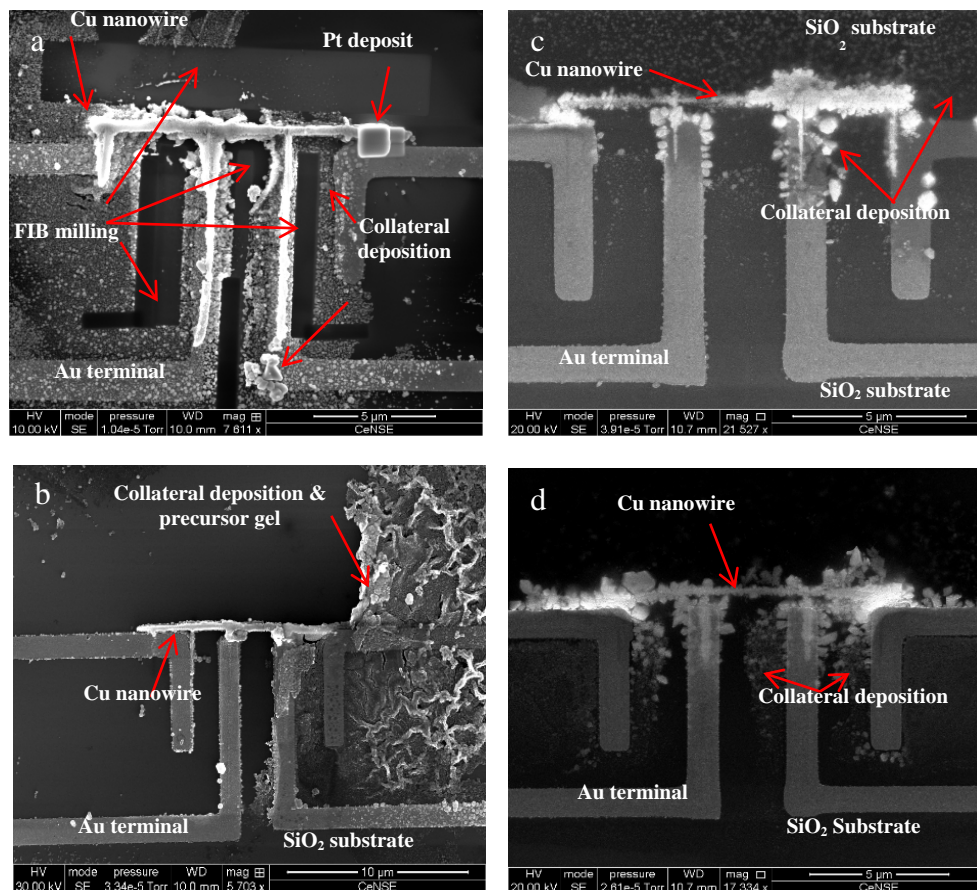
Figure 5-2: Micrographs of successful nanowire deposits. Solution residue and unwanted collateral deposition are visible around all wires. (a) Precursor used: 0.25M CuSO4+ 0.1M H2SO4+ 100ppm PEG 1000. FIB was used to ensure there were no alternative current paths, as well as deposit platinum on the right end of the copper wire to ensure good electrical contact. (b) Precursor used: 0.25M $CuSO_4$+ 0.1M H_2SO_4+ 1mM Triton X-100. (c – d) Precursor used: 0.25M $CuSO_4$+ 0.1M H_2SO_4+ 8mM SDS.

Table 5-1: Patterning conditions dimensions of nanowires, and extracted resistivity. The dimensions of nanowires were averaged from three measurements each.

Line	Acc. voltage (kV)	Pressure (Torr)	Beam Current (pA)	Dose (μC/cm)	Length (μm)	x-sectional area (μm^2)	Resistance (Ω)	**Resistivity (μΩ•cm)**
a	30	5.7	550	25	3.3	0.76	210	**5000**
b	30	5.7	550	20	2.9	0.36	63	**800**
c	30	5.5	683	20	3.6	0.36	37	**370**
d	30	5.5	1286	10 × 5 loops	3.7	0.45	5.5	**67**

The results from figure (5-2) and table (5-1) show drastic improvements in resistivity of LP-EBID of copper compared to previous resistivity results from gas-phase EBID. As mentioned in chapter 3, EBID of copper from Cu(II)(hfac)$_2$ resulted in a resistivity of ~10 kΩ•cm and dropped to 1 Ω•cm after post-processing anneal [11, 12]. The results in table (5-1) are at least 5-6 orders of magnitude lower than that of as-deposited copper from gas phase reactants and at least 2-3 orders of magnitude lower than that of annealed materials. Furthermore, the lowest resistivity, corresponding to line (d) in table (5-1), is only 1 order of magnitude higher compared to the bulk resistivity of copper, which is 1.68 μΩ•cm. Note, as mentioned in chapter 3, one early study reported a resistivity of 3.6 μΩ•cm using the gaseous precursor (hfa)Cu-VTMS[36], but this has not been borne out in later work. Figure (5-3) shows an I-V graph that corresponds to the resistance of the nanowire in figure (5-2d) generated from the MATLAB interface with the four point probe. Figure (5-4) is an energy dispersive x-ray (EDX) analysis taken from the center of the nanowire in figure (5-2d). Although figure (5-4) is not meant to provide accurate data on copper content in the deposit, it confirms the presence of copper in the deposit.

As can be seen from the micrographs of the deposits, the pattern fidelity of the lines is limited by collateral deposition of copper and precipitation of the additives near the patterns. In figure (5-2a) FIB milling was used in order to clean the areas between the gold electrodes to ensure that the only current path is through the nanowire. The platinum square was deposited using EBID to ensure good contact between the wire and the right

current electrode. The right side of figure (5-2b) shows precursor droplet solidification in what appears to be a gel. Recall that in chapter 3, it was mentioned that Triton can form an insoluble gel if its concentration becomes high, which could explain the state of the precursor in this case. Finally, figure (5-2c,d) stress the issue of collateral deposition around the deposit. Even though there is strong evidence that LP-EBID produces highly conductive deposits, it is important to acknowledge the lack of repeatability in the results of LP-EBID. The number of variables that affect LP-EBID, such as electron-precursor interaction, precursor concentration, precursor chemistry, microdroplet profile, wetting process, scanning techniques, beam parameters, etc. calls for further research to isolate each variable and study its effect on deposit properties. Once issues like the precursor precipitate and collateral deposition are resolved, LP-EBID will play a serious role in the various applications of EBID.
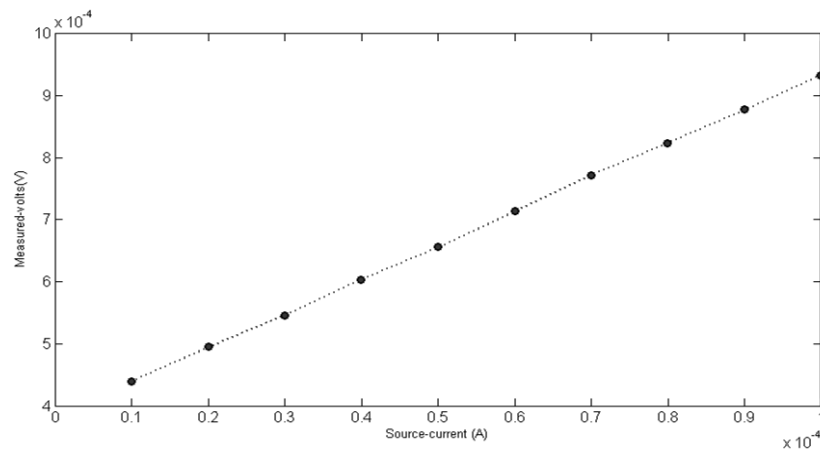
Figure 5-3: I-V curve for current interval of 1 mA-10 mA for wire in figure (5-2d). The resistance of the wire is determined by finding the slope of the I-V curve.
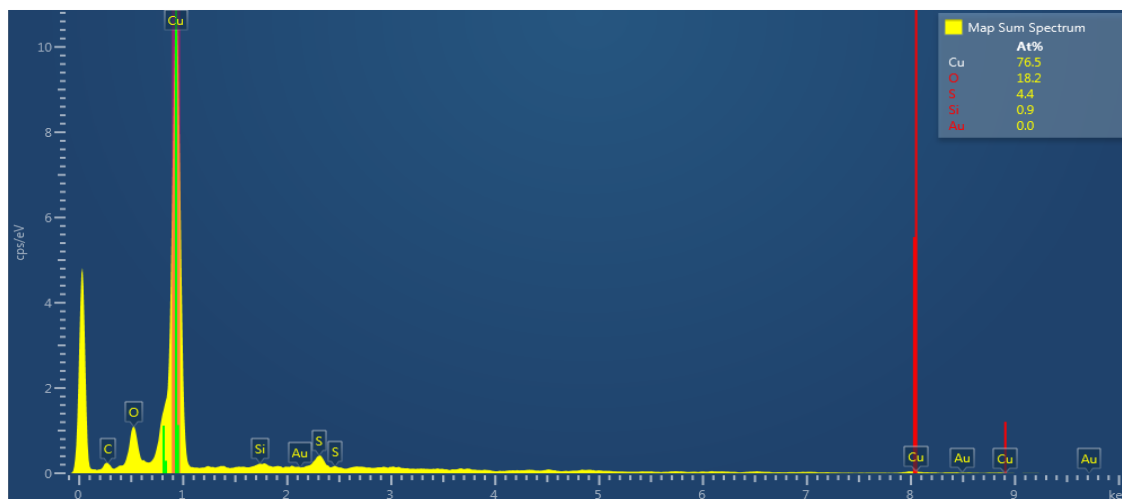
Figure 5-4: EDX spectrum of the center of wire (d) from figure (5-2). The peaks around 0.9 and 8 correlate to copper's Lα and Kα peaks.

5.2 Interesting Observations

In this section, I will highlight a couple of interesting observations that surfaced throughout this work. The first observation is illustrated in figure (5-5) below, where copper deposition is significantly reduced or totally absent on the gold electrodes, forming a discontinuous nanowire. The fact that the line is continuous everywhere else, except on the electrodes, verifies that there are sufficient copper ions in the precursor for deposition, as shown in figure (5-6). There are two possible explanations for this phenomenon. First, it may be that the precursor droplet does not wet the gold regions. Nobel metals exposed to laboratory environments rapidly adsorb hydrocarbons and become hydrophobic. Thus, the hydrophobicity of the gold could increase between the sample preparation process and deposition process. Wetting may be further prevented by pinning of the droplet edge on the gold electrodes which stand 35 nm above the substrate. However, plasma cleaning the sample and the addition of surfactant should mitigate these concerns. An alternative explanation is that the copper deposits do not readily nucleate on the gold surface, or that the deposition rate is greatly reduced on gold. This is conceivable if an electrochemical mechanism is responsible for nucleation and/or growth given that the potential of the gold electrode could be quite different from the locally charged SiO_2. A way to work around this issue is to deposit the nanowire above the

electrodes using the pattern generator, and then manually scan connectors between the nanowire and the electrodes until good connections are insured.
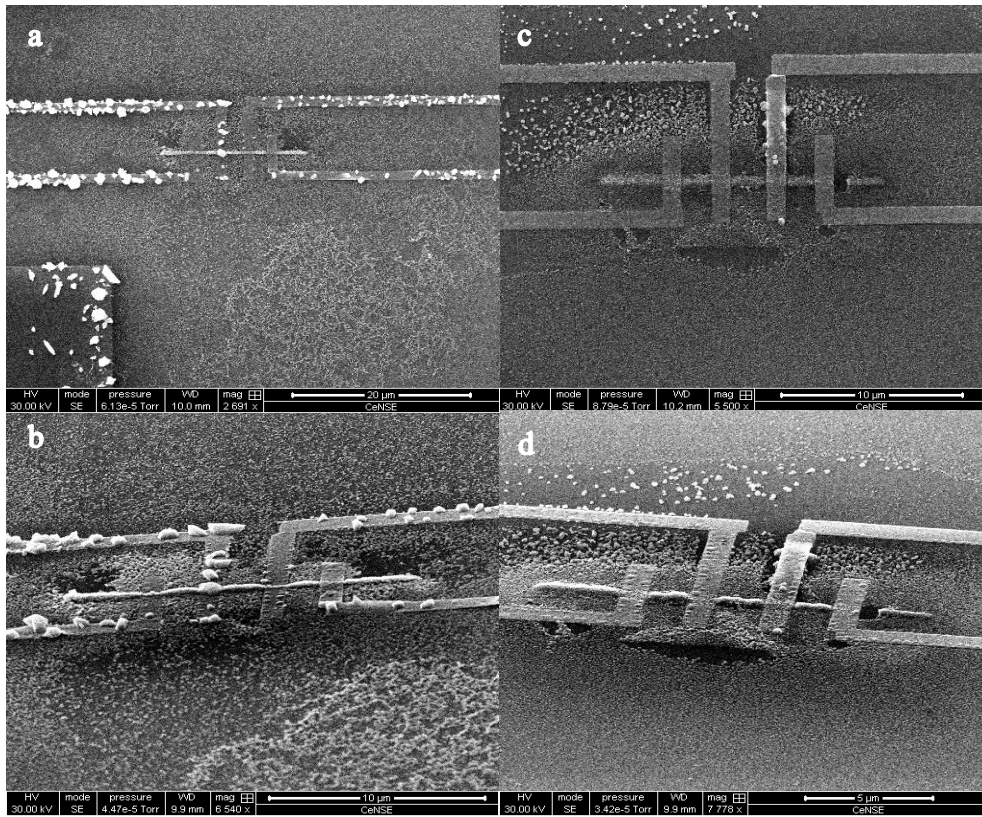
Figure 5-5: Micrographs of two copper nanowires deposited via LP-EBID that show discontinuity of the wire over the gold electrodes. (a,c)top view of nanowires. (b,d) 60° tilt view of nanowires.
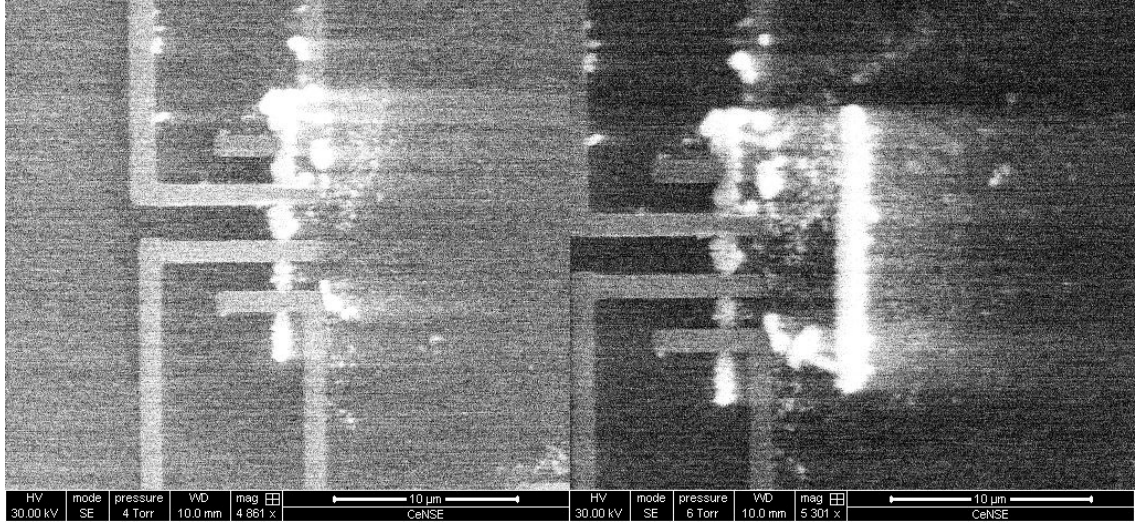
Figure 5-6: Micrograph of nanowire deposited via LP-EBID illustrating the issue with copper deposition on gold. The fact that a continuous line is achieved close to the discontinuous line shows evidence that enough copper ions are available for deposition in the proximity of the gold electrodes.

Another interesting observation is illustrated in figure (5-7). In figure (5-7a), after performing a dot exposure, the precursor was seen to expand around the exposed area. This effect is seen more pronounced in figure (5-7b), where the droplet followed the beam scan for a significant distance. A possible explanation for this phenomenon is electrowetting. Since the oxide layer is not conductive, the electron beam could induce a local charge around the irradiated area, causing the liquid to expand in the direction of the beam scan. This phenomenon has been seen before [32] and was mentioned in chapter (3). Upon reflecting on this effect, electrowetting can be exploited to drive the precursor liquid where deposition is needed.
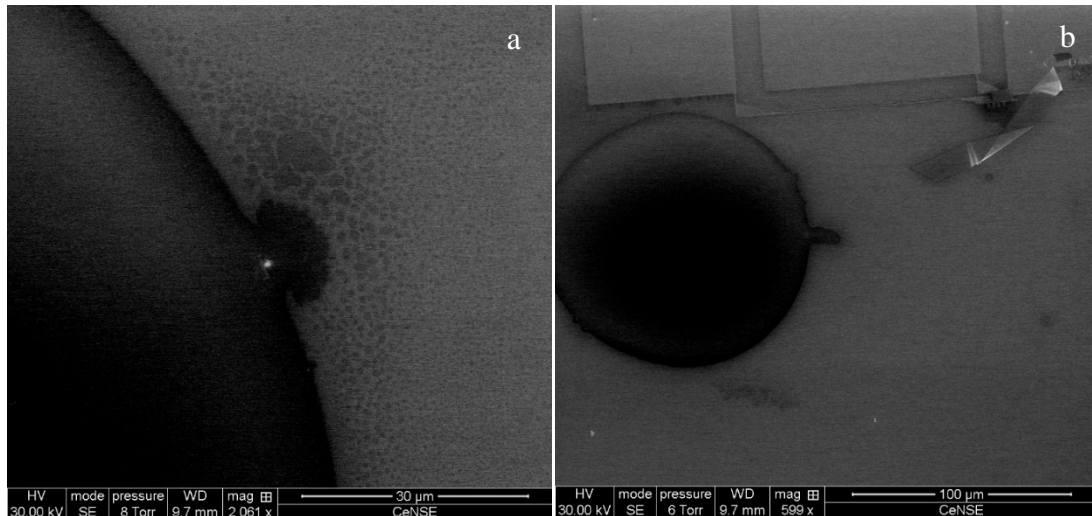
Figure 5-7: Micrograph of a copper precursor droplet showing the effect of beam scan on the liquid edge. (a) After performing a dot exposure, the precursor expanded around the deposit. (b) Top view of the precursor droplet following the beam after scanning the beam in one direction for a certain distance.

5.3 Summary and Conclusion

This thesis introduced the importance of Liquid-Phase Electron Beam Induced Deposition in today's advancements with industries such as the Integrated Circuits (IC) industry, and highlighted the importance of copper as the future material for interconnects. A literature review of EBID and LP-EBID established how EBID impacts diverse applications, and focused the attention on the need for a refined patterning technique that achieves higher purity deposits, of which LP-EBID proves to be a strong candidate. The goal of this work was to assess the resistivity of LP-EBID of copper nanowires and compare the findings with similar results from the literature of EBID. A detailed experimental process was provided and promising results were discussed.

The results from this work provide further evidence that LP-EBID results in highly conductive deposits. The best achieved resistivity of the deposited copper was 67 μΩ•cm, which is one order of magnitude higher than bulk resistivity. The overall resistivity analysis from LP-EBID of copper shows at least 5-6 orders of magnitude improvement in resistivity compared to as-deposited copper from gas-phase EBID, and at least 2-3 orders of magnitude improvement compared to annealed materials. The low resistivity of LP-

43

EBID deposits without post-processing highlights the importance of further research to overcome challenges associated with deposition via liquid precursors, such as collateral deposition; local delivery of the reactant; precursors precipitate; and control of liquid thickness. Further advancement in LP-EBID could improve the quality of existing EBID applications, enhance the literature on electron-fluid interactions, and open new doors in the field of nanofabrication. It is one step closer in the path of creating pure material nanostructures that can be produced according to user-defined specifications.

Appendix – MATLAB code for four point probe

```
% function automation()
clear all
delete(instrfindall)
obj1 = serial('COM3');
% % Reduce timeout to 1 second (default is 10 seconds)
obj1.Timeout = 1;
fopen(obj1);
fprintf(obj1, '++addr 24');
fprintf(obj1, '++mode 1');
fprintf(obj1, '++auto 0');
fprintf(obj1,'++eoi 1');
fprintf(obj1,'++eos 0');
fprintf(obj1,'++eot_enable 1');
fprintf(obj1,'++eot_char 22');
% fprintf(obj1, '*WAI');
% fprintf(obj1,':*RST');
fprintf(obj1, '*IDN?');
% fprintf(obj1, '*WAI');
fprintf(obj1, '++read eoi');
id = fread(obj1);
%
% % Display id
disp(sprintf('%c', id));
fprintf(obj1,':*RST');
% setup the 2400 to generate an SRQ on buffer full
fprintf(obj1,':*ESE 0');
fprintf(obj1,':*CLS');
fprintf(obj1,':STAT:MEAS:ENAB 512');
fprintf(obj1,':*SRE 1');
% buffer set up
fprintf(obj1,':TRAC:CLE');
fprintf(obj1,':TRAC:POIN 10'); % buffer size
% Set up the Sweep
fprintf(obj1,':SOUR:FUNC:MODE CURR');
fprintf(obj1,':SOUR:CURR:STAR 0.0001');
fprintf(obj1,':SOUR:CURR:STOP 0.001');
fprintf(obj1,':SOUR:CURR:STEP 0.0001');
fprintf(obj1,':SOUR:CLE:AUTO ON');
fprintf(obj1,':SOUR:CURR:MODE SWE');
fprintf(obj1,':SOUR:SWE:SPAC LIN');
fprintf(obj1,':SOUR:DEL:AUTO OFF');
fprintf(obj1,':SOUR:DEL 0');
fprintf(obj1,':SENS:FUNC "VOLT"');
fprintf(obj1,':SENS:FUNC:CONC ON');
fprintf(obj1,':SENS:VOLT:RANG:AUTO ON');
%%%%%%%%%%%%%%%%%%%%%%%%%%%%%%%%%%%%%%%%
% IMPORTANT: if the unit goes into compliance,
% adjust the compliance or the range value
```

```
%fprintf(obj1,':SENS:VOLT:PROT:LEV 20'); % voltage compliance
%fprintf(obj1,':SENS:VOLT:RANG 20'); % volt measurement range
%%%%%%%%%%%%%%%%%%%%%%%%%%%%%%%%%%%%%%%%
fprintf(obj1,':SENS:VOLT:NPLC 1');
fprintf(obj1,':FORM:ELEM:SENS VOLT,CURR');
fprintf(obj1,':TRIG:COUN 10');
fprintf(obj1,':TRIG:DEL 0');
fprintf(obj1,':SYST:AZER:STAT OFF');
fprintf(obj1,':SYST:TIME:RES:AUTO ON');
fprintf(obj1,':TRAC:TST:FORM ABS');
fprintf(obj1,':TRAC:FEED:CONT NEXT');
fprintf(obj1,':OUTP ON');
fprintf(obj1,':INIT');
%
% fprintf(obj1,'++spoll');
% fprintf(obj1,'++srq');
fprintf(obj1,':TRAC:DATA?');
fprintf(obj1, '++read eoi');
A = scanstr(obj1,',','%f');
V=A(1:2:length(A));
C=A(2:2:length(A));
plot(C,V,':bo','LineWidth',0.5,...
'MarkerEdgeColor','k',...
'MarkerFaceColor','r',...
'MarkerSize',5)
xlabel('Source-current (A)'),ylabel('Measured-volts(V)')
title('Keithley 2400: Sweeps I (.1mA-1mA) & Measure V');
fprintf(obj1,'*RST')
fprintf(obj1,':*CLS')
fprintf(obj1,':*SRE 0')
% make sure STB bit is 0
fclose(obj1)
delete(obj1)
```

References

[1]   N. Silvis-Cividjian, C. Hagen, P. v. d. Kruit, M. vd Stam, and H. Groen, "Direct fabrication of nanowires in an electron microscope," *Applied Physics Letters,* vol. 82, pp. 3514-3516, 2003.

[2]   V. Gopal, E. A. Stach, V. R. Radmilovic, and I. A. Mowat, "Metal delocalization and surface decoration in direct-write nanolithography by electron beam induced deposition," *Applied physics letters,* vol. 85, pp. 49-51, 2004.

[3]   K. Mølhave, D. N. Madsen, A. M. Rasmussen, A. Carlsson, C. C. Appel, M. Brorson*, et al.*, "Solid gold nanostructures fabricated by electron beam deposition," *Nano Letters,* vol. 3, pp. 1499-1503, 2003.

[4]   S. Rubel, M. Trochet, E. Ehrichs, W. F. Smith, and A. De Lozanne, "Nanofabrication and rapid imaging with a scanning tunneling microscope," *Journal of Vacuum Science & Technology B,* vol. 12, pp. 1894-1897, 1994.

[5]   Y. Lau, P. Chee, J. Thong, and V. Ng, "Properties and applications of cobalt-based material produced by electron-beam-induced deposition," *Journal of Vacuum Science & Technology A,* vol. 20, pp. 1295-1302, 2002.

[6]   Z. Liu, K. Mitsuishi, and K. Furuya, "Features of self-supporting tungsten nanowire deposited with high-energy electrons," *Journal of applied physics,* vol. 96, pp. 619-623, 2004.

[7]   T. Liang, E. Frendberg, B. Lieberman, and A. Stivers, "Advanced photolithographic mask repair using electron beams," *Journal of Vacuum Science & Technology B,* vol. 23, pp. 3101-3105, 2005.

[8]   X. Yang, M. Simpson, S. Randolph, P. Rack, L. Baylor, H. Cui*, et al.*, "Integrated tungsten nanofiber field emission cathodes selectively grown by nanoscale electron beam-induced deposition," *Applied Physics Letters,* vol. 86, p. 183106, 2005.

[9]   A. Perentes, A. Bachmann, M. Leutenegger, I. Utke, C. Sandu, and P. Hoffmann, "Focused electron beam induced deposition of a periodic transparent nano-optic pattern," *Microelectronic engineering,* vol. 73, pp. 412-416, 2004.

[10]   A. Luisier, I. Utke, T. Bret, F. Cicoira, R. Hauert, S.-W. Rhee*, et al.*, "Comparative Study of Cu-Precursors for 3D Focused Electron Beam Induced Deposition [J. Electrochem. Soc., 151, C535 (2004)][J. Electrochem. Soc., 151, C590 (2004)]," *Journal of The Electrochemical Society,* vol. 152, pp. L1-L1, 2005.

[11]   A. Szkudlarek, A. R. Vaz, Y. Zhang, A. Rudkowski, C. Kapusta, R. Erni*, et al.*, "Formation of pure Cu nanocrystals upon post-growth annealing of Cu–C material obtained from focused electron beam induced deposition: comparison of different methods," *Beilstein journal of nanotechnology,* vol. 6, pp. 1508-1517, 2015.

[12]   A. Szkudlarek, A. R. Vaz, Y. Zhang, A. Rudkowski, C. Kapusta, R. Erni*, et al.*, "Correction: Formation of pure Cu nanocrystals upon post-growth annealing of Cu–C material obtained from focused electron beam induced deposition: comparison of different methods," *Beilstein Journal of Nanotechnology,* vol. 6, pp. 1935-1936, 2015.

[13]   W. Van Dorp and C. Hagen, "A critical literature review of focused electron beam induced deposition," *Journal of Applied Physics,* vol. 104, p. 081301, 2008.

[14]   E. U. Donev and J. T. Hastings, "Electron-beam-induced deposition of platinum from a liquid precursor," *Nano letters,* vol. 9, pp. 2715-2718, 2009.

[15]   M. Bresin, A. Chamberlain, E. U. Donev, C. B. Samantaray, G. S. Schardien, and J. T. Hastings, "Electron-Beam-Induced Deposition of Bimetallic Nanostructures from Bulk Liquids," *Angewandte Chemie,* vol. 125, pp. 8162-8165, 2013.

[16]   M. Bresin, A. Botman, S. J. Randolph, M. Straw, and J. T. Hastings, "Liquid phase electron-beam-induced deposition on bulk substrates using environmental scanning electron microscopy," *Microscopy and Microanalysis,* vol. 20, pp. 376-384, 2014.

[17]   M. Bresin, A. Botman, S. J. Randolph, M. Straw, and J. T. Hastings, "Liquid phase electron-beam-induced deposition on bulk substrates using environmental scanning electron microscopy," *Microscopy and Microanalysis,* vol. 20, p. 376, 2014.

[18]   S. E. L. B. J. T. Hastings, "Focused Electron Beam Induced Deposition ofCopper with High Resolution and Purity from Aqueous Solutions," *Nanotechnology,* Forthcoming 2016.

[19]   R. L. Stewart, "Insulating films formed under electron and ion bombardment," *Physical review,* vol. 45, p. 488, 1934.

[20]   A. Ennos, "The sources of electron-induced contamination in kinetic vacuum systems," *British Journal of Applied Physics,* vol. 5, p. 27, 1954.

[21]   R. W. Christy, "Formation of thin polymer films by electron bombardment," *Journal of Applied Physics,* vol. 31, pp. 1680-1683, 1960.

[22]   N. Silvis-Cividjian and C. W. Hagen, "Electron-Beam–Induced Nanometer-Scale Deposition," *Advances in Imaging and Electron Physics,* vol. 143, pp. 1-235, 2006.

[23]   A. Broers, W. Molzen, J. Cuomo, and N. Wittels, "Electron-beam fabrication of 80-Å metal structures," *Applied Physics Letters,* vol. 29, pp. 596-598, 1976.

[24]   S. Randolph, J. Fowlkes, and P. Rack, "Focused, nanoscale electron-beam-induced deposition and etching," *Critical Reviews in Solid State and Materials Sciences,* vol. 31, pp. 55-89, 2006.

[25]   A. Luisier, I. Utke, T. Bret, F. Cicoira, R. Hauert, S.-W. Rhee*, et al.*, "Comparative study of Cu-precursors for 3D focused electron beam induced deposition," *Journal of The Electrochemical Society,* vol. 151, pp. C590-C593, 2004.

[26]   Reprinted from *Microelectronic engineering,* vol. 78, T. Bret, I. Utke, and P. Hoffmann, "Influence of the beam scan direction during focused electron beam induced deposition of 3D nanostructures," pp. 307-313, Copyright (2005), with permission from Elsevier.

[27]   A. Botman, J. Mulders, and C. Hagen, "Creating pure nanostructures from electron-beam-induced deposition using purification techniques: a technology perspective," *Nanotechnology,* vol. 20, p. 372001, 2009.

[28]   K. T. Kohlmann-von Platen, L. M. Buchmann, H. C. Petzold, and W. H. Brünger, "Electron-beam induced tungsten deposition: Growth rate enhancement and applications in microelectronics," *Journal of Vacuum Science & Technology B,* vol. 10, pp. 2690-2694, 1992.

[29]   N. A. Roberts, J. D. Fowlkes, G. A. Magel, and P. D. Rack, "Enhanced material purity and resolution via synchronized laser assisted electron beam induced deposition of platinum," *Nanoscale,* vol. 5, pp. 408-415, 2013.

[30]   M. M. Shawrav, P. Taus, H. D. Wanzenboeck, M. Schinnerl, M. Stöger-Pollach, S. Schwarz*, et al.*, "Highly conductive and pure gold nanostructures grown by electron beam induced deposition," *Scientific Reports,* vol. 6, 2016.

[31]   M. den Heijer, I. Shao, A. Radisic, M. C. Reuter, and F. M. Ross, "Patterned electrochemical deposition of copper using an electron beam," *APL Materials,* vol. 2, p. 022101, 2014.

[32]   S. J. Randolph, A. Botman, and M. Toth, "Capsule-free fluid delivery and beam-induced electrodeposition in a scanning electron microscope," *RSC Advances,* vol. 3, pp. 20016-20023, 2013.

[33]   G. Schardein, E. Donev, and J. Hastings, "Electron-beam-induced deposition of gold from aqueous solutions," *Nanotechnology,* vol. 22, p. 015301, 2010.

[34]   J. Tao, N. W. Cheung, and C. Hu, "Electromigration characteristics of copper interconnects," *IEEE Electron Device Letters,* vol. 14, pp. 249-251, 1993.

[35]   Y. Ochiai, J. i. Fujita, and S. Matsui, "Electron-beam-induced deposition of copper compound with low resistivity," *Journal of Vacuum Science & Technology B,* vol. 14, pp. 3887-3891, 1996.

[36] Y. Ochiai, J. i. Fujita, and S. Matsui, "Electron-beam-induced deposition of copper compound with low resistivity," *Journal of Vacuum Science & Technology B,* vol. 14, pp. 3887-3891, 1996.

[37] H. Miyazoe, I. Utke, H. Kikuchi, S. Kiriu, V. Friedli, J. Michler*, et al.*, "Improving the metallic content of focused electron beam-induced deposits by a scanning electron microscope integrated hydrogen-argon microplasma generator," *Journal of Vacuum Science & Technology B,* vol. 28, pp. 744-750, 2010.

[38] T. Chiang, H. Sawin, and C. Thompson, "Ion-induced chemical vapor deposition of high purity Cu films at room temperature using a microwave discharge H atom beam source," *Journal of Vacuum Science & Technology A,* vol. 15, pp. 2677-2686, 1997.

[39] S.-E. Lai, Y.-J. Hong, Y.-T. Chen, Y.-T. Kang, P. Chang, and T.-R. Yew, "Direct-Writing of Cu Nano-Patterns with an Electron Beam," *Microscopy and Microanalysis,* vol. 21, pp. 1639-1643, 2015.

[40] M. Massucci, S. L. Clegg, and P. Brimblecombe, "Equilibrium vapor pressure of H2O above aqueous H2SO4 at low temperature," *Journal of Chemical & Engineering Data,* vol. 41, pp. 765-778, 1996.

[41] L. Boehme, M. Bresin, A. Botman, J. Ranney, and J. T. Hastings, "Focused electron beam induced etching of copper in sulfuric acid solutions," *Nanotechnology,* vol. 26, p. 495301, 2015.

[42] I. Enculescu, Z. Siwy, D. Dobrev, C. Trautmann, M. T. Molares, R. Neumann*, et al.*, "Copper nanowires electrodeposited in etched single-ion track templates," *Applied Physics A,* vol. 77, pp. 751-755, 2003.

[43] A. Noubani, "Resistivity of Copper Nanowires Deposited by Liquid-Phase Electron Beam Induced Deposition," University of Kentucky, Unpublished Project Report, 2014.

Vita

Amjad Syam was born in Amman, Jordan. He received his B.S in Electrical Engineering, Summa Cum Laude, from the University of Kentucky in Lexington, KY. In 2015, He received a Teaching Assistantship from the ECE department at the University of Kentucky and pursued a Master of Science (M.Sc) degree in Electrical Engineering.